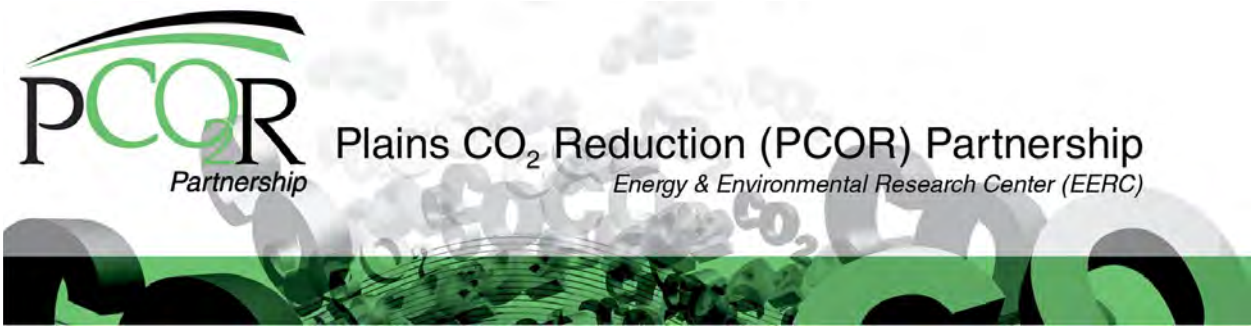

TECHNICAL APPROACHES TO STACKED STORAGE: GEOMECHANICS SUPPLEMENT

Plains CO_2 Reduction (PCOR) Partnership Initiative
Task 2 – Deliverable D3.B – Revision

Prepared for:

Joshua Hull

National Energy Technology Laboratory
U.S. Department of Energy
626 Cochrans Mill Road
PO Box 10940
Pittsburgh, PA 15236-0940

Cooperative Agreement No. DE-FE0031838

Prepared by:

Matthew L. Belobraydic
Thomas H. Jo
Fazilatun N. Mahmood
Bret J. Fossum
Santosh Patil
Jun He
Todd Jiang
Remington M. Leger
Chantsalmaa Dalkhaa
Nicholas W. Bosshart
Kevin C. Connors

Energy & Environmental Research Center
University of North Dakota
15 North 23rd Street, Stop 9018
Grand Forks, ND 58202-9018

2022-EERC-05-01

May 2022

EERC DISCLAIMER

LEGAL NOTICE This research report was prepared by the Energy & Environmental Research Center (EERC), an agency of the University of North Dakota, as an account of work sponsored by the U.S. Department of Energy (DOE). Because of the research nature of the work performed, neither the EERC nor any of its employees makes any warranty, express or implied, or assumes any legal liability or responsibility for the accuracy, completeness, or usefulness of any information, apparatus, product, or process disclosed or represents that its use would not infringe privately owned rights. Reference herein to any specific commercial product, process, or service by trade name, trademark, manufacturer, or otherwise does not necessarily constitute or imply its endorsement or recommendation by the EERC.

ACKNOWLEDGMENT

This material is based upon work supported by DOE's National Energy Technology Laboratory under Award No. DE-FE0031838 and the North Dakota Industrial Commission (NDIC) under Contract Nos. FY20-XCI-226 and G-050-96.

DOE DISCLAIMER

This report was prepared as an account of work sponsored by an agency of the United States Government. Neither the United States Government, nor any agency thereof, nor any of their employees, makes any warranty, express or implied, or assumes any legal liability or responsibility for the accuracy, completeness, or usefulness of any information, apparatus, product, or process disclosed, or represents that its use would not infringe privately owned rights. Reference herein to any specific commercial product, process, or service by trade name, trademark, manufacturer, or otherwise does not necessarily constitute or imply its endorsement, recommendation, or favoring by the United States Government or any agency thereof. The views and opinions of authors expressed herein do not necessarily state or reflect those of the United States Government or any agency thereof.

NDIC DISCLAIMER

This report was prepared by the Energy & Environmental Research Center (EERC) pursuant to an agreement partially funded by the Industrial Commission of North Dakota, and neither the EERC nor any of its subcontractors nor the North Dakota Industrial Commission nor any person acting on behalf of either:

(A) Makes any warranty or representation, express or implied, with respect to the accuracy, completeness, or usefulness of the information contained in this report or that the use of any information, apparatus, method, or process disclosed in this report may not infringe privately owned rights; or

(B) Assumes any liabilities with respect to the use of, or for damages resulting from the use of, any information, apparatus, method, or process disclosed in this report.

Reference herein to any specific commercial product, process, or service by trade name, trademark, manufacturer, or otherwise does not necessarily constitute or imply its endorsement, recommendation, or favoring by the North Dakota Industrial Commission. The views and opinions of authors expressed herein do not necessarily state or reflect those of the North Dakota Industrial Commission.

TABLE OF CONTENTS

LIST OF FIGURES

Continued . . .

LIST OF FIGURES (continued)

LIST OF TABLES

TECHNICAL APPROACHES TO STACKED STORAGE: GEOMECHANICS SUPPLEMENT

EXECUTIVE SUMMARY

When two or more carbon dioxide (CO_2) storage targets are present in the subsurface at the same geographic location, a CO_2 storage project may pursue a stacked storage approach. The potential geomechanical effects of injection in multiple intervals on interburden and on the cap rock of the uppermost injection interval are not well understood. This investigation assessed the geomechanical effects of stacked storage by modeling the combined stresses and pore pressure changes to generate a general understanding of stresses placed on interburden between CO_2 storage formations and the uppermost seal.

With the potential for each storage complex to impact another in a stacked storage scenario (e.g., hydraulic communication and geomechanical failure), a workflow was implemented to analyze the dynamic changes of stress utilizing a single 3D model with three scenarios. The workflow integrates the efforts of static geologic modeling, dynamic numerical simulation, and mechanical earth modeling to identify the effective stress evolution, generated thermal stress, and predicted locations of potential shear and tensile failure of the interburden and overburden associated with the injection of CO_2 in the subsurface. Identification of changes in stress for storage reservoirs, interburden, and uppermost seal improves our understanding of the risks associated with injection and long-term containment of CO_2. The geomechanical workflow is applicable for forward-modeling induced stresses for any CO_2 storage project including saline aquifers, enhanced oil recovery opportunities, or unconventional reservoirs and can accommodate any number of stacked storage formations within a stratigraphic sequence. The present workflow, however, does not consider faulting and fractures and the potential for failure of critically stressed faults or fractures in response to CO_2 injection.

Numerous potential scenarios with many variables could be considered in geomechanical investigations, but this case study focused on a simplified stacked storage scenario to generate initial learnings in two data-rich saline reservoirs and to generate a series of technical and risking elements that should be considered when evaluating the potential for stacked storage. This stacked storage case study was focused on the Broom Creek and Inyan Kara Formations. A static geologic model was constructed for a small region within the Williston Basin from the ground surface down to the Amsden Formation below the Broom Creek. This geologic model was used to perform three dynamic numerical simulation cases to test the geomechanical effects of injecting the operational maximum CO_2 volume over a 20-year period into each formation: stand-alone Inyan Kara

injection, stand-alone Broom Creek injection, and simultaneous Inyan Kara and Broom Creek injection with two separate wells.

Geomechanical modeling was carried out utilizing a two-part mechanical earth modeling process: 1) 1D wellbore analysis and 2) 3D field-scale analysis. The 1D mechanical earth models (MEMs) were completed along key wellbores to derive dynamic and static constitutive properties, overburden stress, maximum horizontal stress, and minimum horizontal stress at the time of drilling and were used to calibrate and propagate the initial stress and rock strength conditions in the 3D MEM. Pore pressure and fluid temperatures for each 20-year injection scenario were forward-modeled to calculate effective stress evolution and thermal stress generated on the stacked storage complex for each time step. In this study, the geomechanical modeling was carried out separately from the dynamic fluid simulation; however, it is recommended as a best practice to carry out a coupled modeling process, which would allow for more robust, holistic, and confident analysis.

Given the model boundary conditions and pressure injection parameters, 3D MEM results demonstrate geomechanical isolation and no pressure communication between the Inyan Kara and Broom Creek Formations, with no shear or tensile fracture failures observed in the interburden or upper confining zone. The isolation between the formations is observable in the effective stress evolution during the 20-year injection period for all simulation cases. Observations for generated thermal stress and predicted locations of shear and tensile failure are isolated to modeled cells directly adjacent to CO_2 injection wells.

With any CO_2 storage project, a robust monitoring, reporting, and verification (MRV) program is essential and required to ensure storage integrity. As new CO_2 storage projects come online, the monitoring data will provide the necessary history-matching injection constraints to calibrate and improve 3D simulation approaches and methods in the future. Additionally, CO_2 storage performance-monitoring tools such as 4D seismic and InSAR (interferometric synthetic aperture radar) will provide additional location and timing calibration points for reservoir and stress conditions during injection and plume growth.

The workflow in this case study assessed the geomechanical impacts and stresses for CO_2 storage in a simulated stacked storage operation scenario targeting the Inyan Kara and Broom Creek Formations from site-specific characterization data. Given the broad range of geology, structural styles, and constitutive properties of potential storage and confining zones across the Plains CO_2 Reduction (PCOR) Partnership region, future work should be broadened to reflect the subsurface diversity and to develop a robust set of risking and ranking criteria for potential stacked storage opportunities. Based on results of this study, main geomechanical risking criteria for a CO_2 injection storage project risk register should focus on 1) rock strength, mechanical stratigraphy and constitutive properties of injection, overburden, and interburden layers; 2) critical stress analysis of mapped faults and fractures that impact the confining and injection zones; and 3) risk management and mitigation.

Application and customization of the 3D simulation workflow to evaluate representative geological scenarios, utilizing results and high-graded criteria to risk and rank potential stacked storage opportunities coupled with robust MRV plans, will guide CO_2 storage managers in recommending suitable and safe stacked storage sites.

TECHNICAL APPROACHES TO STACKED STORAGE: GEOMECHANICS SUPPLEMENT

INTRODUCTION

The Plains CO_2 Reduction (PCOR) Partnership is one of four Regional Carbon Sequestration Partnership (RCSP) projects operating under the U.S. Department of Energy (DOE) National Energy Technology Laboratory (NETL) Regional Initiative to Accelerate CCUS (carbon capture, utilization, and storage). The PCOR Partnership region encompasses ten U.S. states and four Canadian provinces in the upper Great Plains and northwestern regions of North America. The PCOR Partnership is led by the Energy & Environmental Research Center (EERC) with support from the University of Wyoming, the University of Alaska Fairbanks, and stakeholders from the public and private sectors. The goal of this joint government–industry effort is to identify and address regional capture, transport, use, and storage challenges facing commercial deployment of CCUS throughout the PCOR Partnership region.

Since 2007, DOE NETL has published several assessments of CO_2 storage resource potential in geologic formations and terrestrial sinks in the United States, with the following geologic reservoirs considered viable targets for CO_2 storage: saline formations, coal seams, conventional hydrocarbon reservoirs, basalt formations, and unconventional oil and gas formations, including shales and tight sands (U.S. Department of Energy National Energy Technology Laboratory, 2015). When two or more storage units are present within the subsurface at the same geographic location, there are opportunities for a CO_2 storage project to use multiple reservoirs as part of an overall storage project (Figure 1). The use of multiple storage reservoirs with overlapping footprints in map view is referred to as stacked storage (Hovorka and others, 2006; Sorensen and others, 2009; Hovorka, 2013).

The PCOR Partnership region has many opportunities for stacked storage in deep saline storage complexes, with CO_2 enhanced oil recovery (EOR) options in hydrocarbon-bearing formations and unconventional reservoirs. Projects within the Powder River Basin, Williston Basin, Denver–Julesburg Basin, and Alberta Basin were reviewed in Belobraydic and others (2021) for stacked storage potential within deep saline aquifers. In general, the saline reservoirs in these basins with the greatest dedicated storage potential in the PCOR Partnership region are mostly sandstone and range in number, depth, thickness, and vertical separation between stacked reservoirs. The approach to carry out a geomechanics analysis of a stacked storage opportunity is identical whether the storage zones are saline aquifer, EOR opportunity, unconventional reservoir, or a combination. The recommended approach is to evaluate stacked storage opportunities in 3D versus 2D. The 3D relationships between constitutive properties, mechanical stratigraphy, and

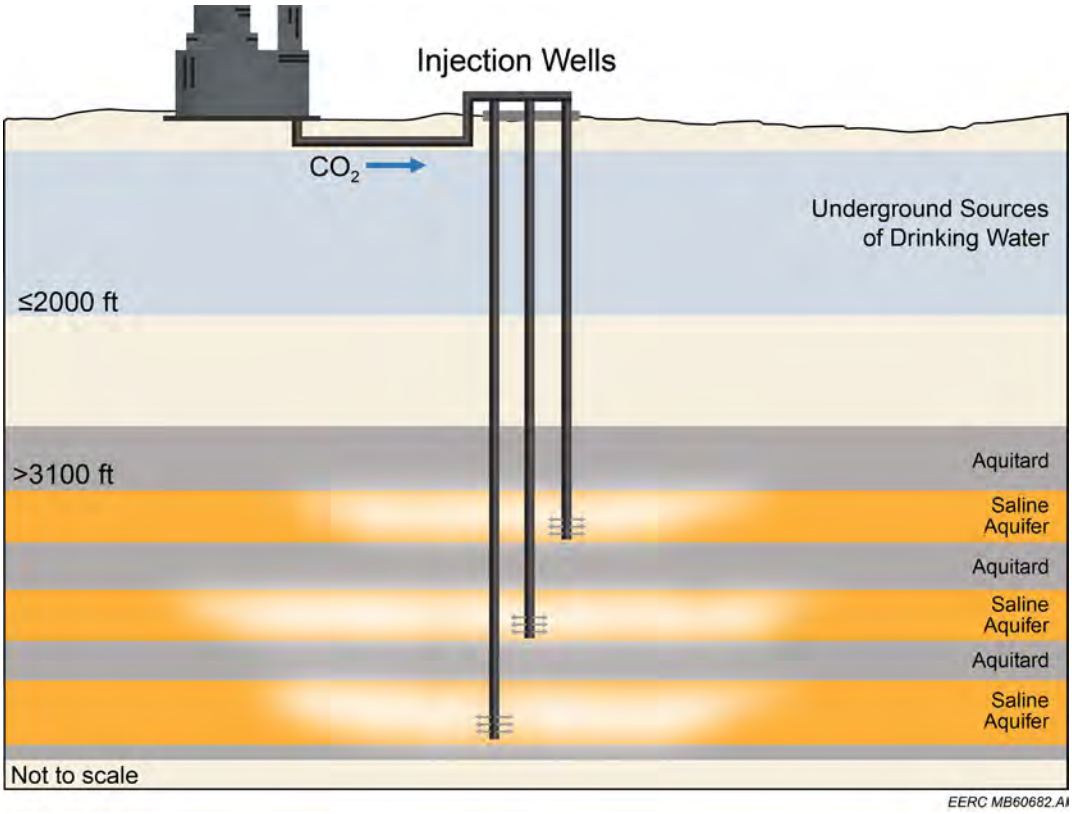

Figure 1. Stacked storage diagram illustrating three saline aquifer storage units separated by aquitard (confining zone) and interburden layers. One stacked storage well pad is depicted from a single capture facility. Distances and depth are not to scale (modified after Belobraydic and others [2021]).

in situ stress state of the injection and confining zones coupled with pertinent structural features can be described, simulated, and used to make informed, risk-based decisions for the selection of suitable stacked storage complexes, along with the design of a robust and site-specific monitoring, reporting, and verification (MRV) plan.

Under a single-formation storage scenario, the geomechanical investigations are generally focused on the storage unit and containment of CO_2 by the surrounding aquitards (i.e., confining zones). However, in the present study considering a stacked storage scenario with multiple storage reservoirs in play, there is potential for each storage complex to affect the others. This geomechanical case study is focused on identifying a general understanding of stresses placed on interburden between CO_2 storage formations and the combined stress placed on the uppermost seal in the absence of faulting or fractures. With the potential for each storage complex to affect another in a stacked storage scenario (e.g., hydraulic communication due to geomechanical failure), a workflow was implemented to analyze the geomechanical impact and stresses in response to CO_2 injection.

The workflow integrates static geologic modeling, numerical flow simulation, and mechanical earth modeling to identify the effective stress evolution, generated thermal stress, and

predicted locations of potential shear and tensile failure modes of injection and confining zones associated with the injection of CO_2 in the subsurface. Modeling changes in stress evolution for storage reservoirs, interburden, and the uppermost seal improved understanding of the storage risks associated with injection and long-term storage of CO_2. The geomechanical workflow is applicable for forward-modeling induced stresses for any CO_2 storage project and can accommodate any number of stacked storage formations within a stratigraphic column.

As a case study, the combined stresses and pore pressure changes associated with multiple formations receiving the operational maximum injection volume of CO_2 for a 20-year period were evaluated for the stacked reservoirs of the Inyan Kara and Broom Creek Formations (Figure 2). These are the shallowest two formations considered for CO_2 injection in the eastern part of the Williston Basin. To estimate overburden stress for the geomechanical investigation, the model extended from the ground surface to below the injection reservoirs. Using the shallowest two reservoirs for this study limited the total stratigraphic section represented in the model. The following inputs were completed to support the geomechanical modeling: 1) geocellular property model from the ground surface down to the Amsden Formation (Figure 2) and 2) numerical flow simulations for maximum operational CO_2 injection over 20 years, including A) stand-alone Inyan Kara CO_2 injection, B) stand-alone Broom Creek CO_2 injection, and C) simultaneous Inyan Kara and Broom Creek CO_2 injection with two separate wells.

Using these results, geomechanical stresses for this stacked storage case study were investigated by combining predicted mechanical properties for rock layers in the storage complex and simulating the effect of CO_2 injection on pore pressure and state of stress for the injection formations, interburden, and upper confining layer. Figure 3 is a positioning map for the well locations and grid boundaries used in this study.

GEOLOGIC MODEL DESCRIPTION AND SIMULATION SCENARIOS

Static Geologic Model Description

A stacked storage case study was built based on the Inyan Kara and Broom Creek Formations of the Williston Basin. A static geologic model representing the two reservoirs was developed to support numerical simulation and geomechanical analysis of a stacked storage system for CO_2 injection and storage. To account for overburden and interburden calculations, the model was constructed using Schlumberger's Petrel E&P software platform (Schlumberger, 2020a) from the ground surface down to the Amsden Formation (Figure 2). The geologic model construction workflow included data collection, data verification, stratigraphic correlation, structural analysis without faulting or fracturing considered, 3D structural grid construction, variography and data analysis, and distributing facies and petrophysical properties.

The Early Cretaceous Inyan Kara Formation is composed of fluvial, estuarine, and marginal marine coarse-to-fine sandstones, siltstones, and shales (Bader, 2017). The Permian Broom Creek Formation is composed of coastal eolian and nearshore marine sandstones and dolomitic sandstones with some interbeds of dolostones and anhydrite (Ziebarth, 1972; Rygh, 1990). The Skull Creek Formation is the upper confining shale layer for the Inyan Kara, and the shales of the

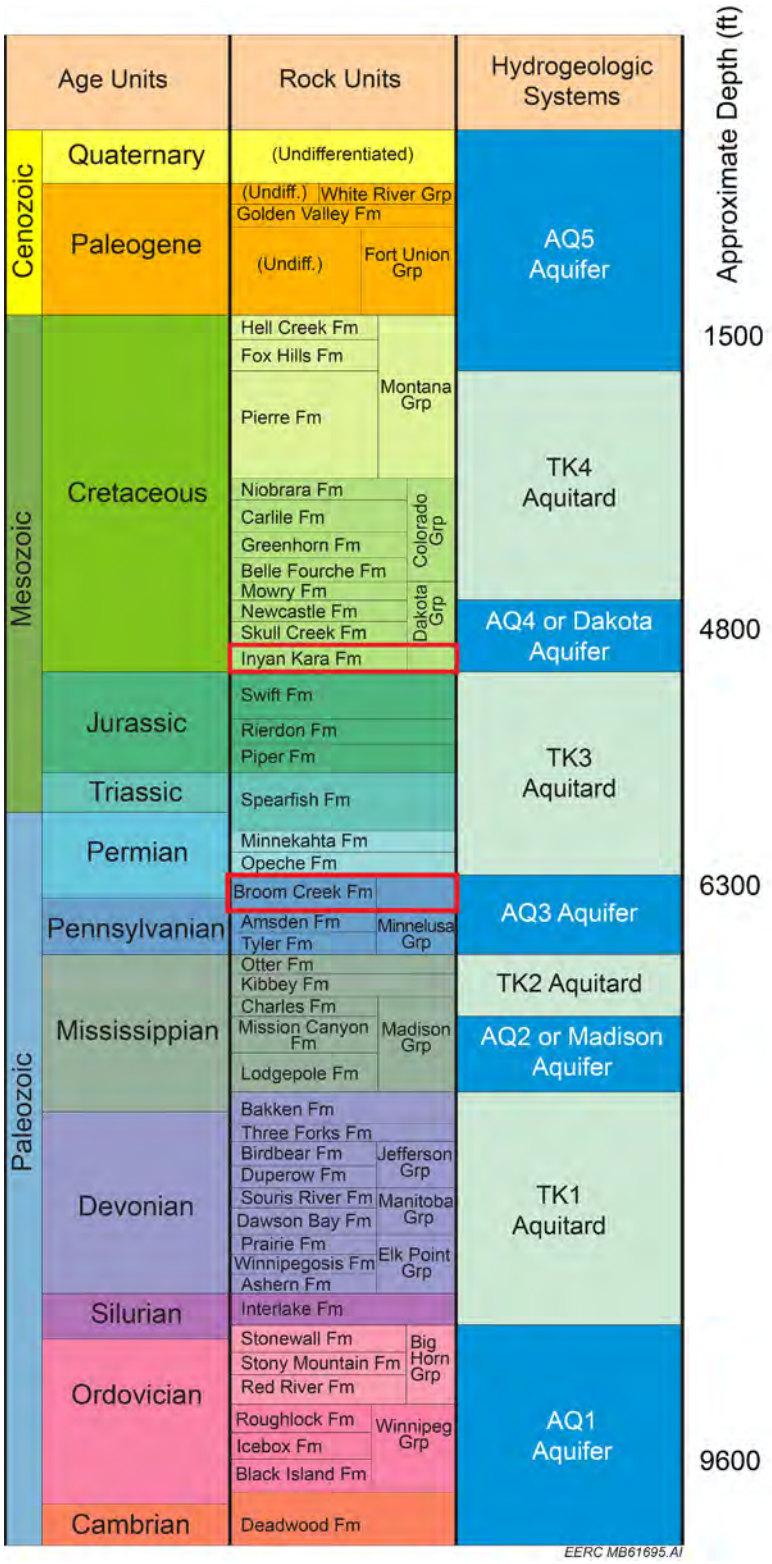

Figure 2. Williston Basin stratigraphic column with major aquifers and aquitards indicated. Red boxes indicate stacked storage targets considered for this study. Depths are approximate for the eastern part of the basin (modified from Peck and others [2020] and Sorensen and others [2009]).

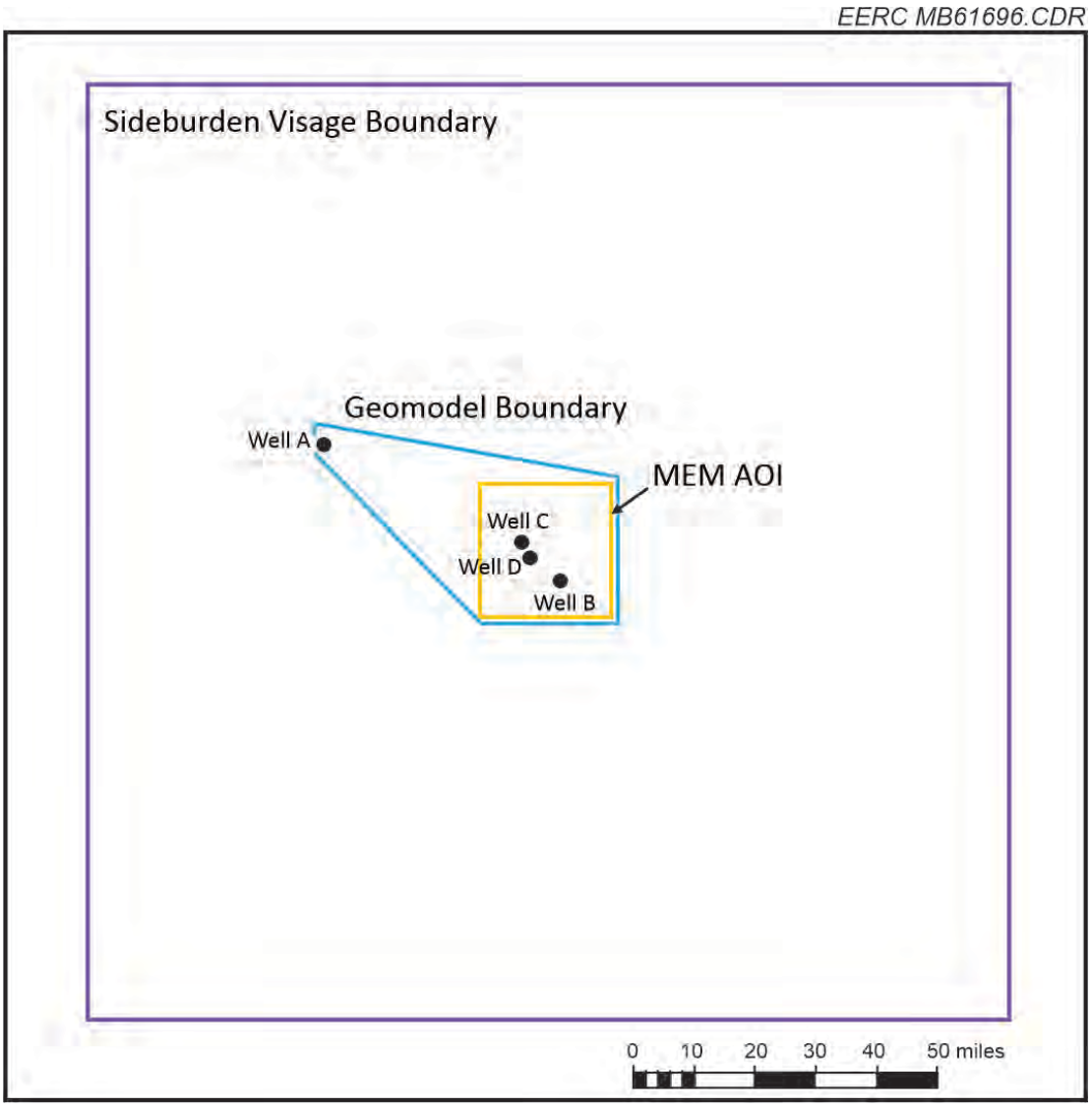

Figure 3. Positioning map showing well locations and grid boundaries used in the study, including the geologic model and simulation boundary (blue), mechanical earth model (MEM) area of interest (AOI) boundary (yellow), and additional volume added in for 3D MEM in Visage representation of sideburden (purple).

Opeche and Spearfish (Piper–Picard members) Formations are the upper confining layer for the Broom Creek Formation. A thick shale interval (~1000 feet) consisting of the Pierre, Greenhorn, and Mowry Formations is the secondary confining zone above the Inyan Kara. These confining formations ensure that any injected CO_2 will be isolated from the lowermost underground source of drinking water in the Fox Hills Formation (Peck and others, 2020). A digital elevation model of the ground surface serves as the top of the model, and the Amsden Formation contour surface shifted down 100 ft (30 m) serves as the base.

Four wells, generically labeled Wells A, B, C, and D (Figure 3), were used to generate data in support of this investigation. The actual location and names of the wells are not important to this case study and have not been included to avoid sensitivities associated with commercial operations. All four wells penetrate through the Broom Creek Formation and contain compressional and shear sonic data necessary for geomechanical modeling. The irregular areal extent for the geologic model allowed for the inclusion of all wells and location of simulated CO_2 injection. The geologic model was 50.5 mi (81.3 km) by 33.1 mi (53.3 km), with an area of 1035 mi^2 (2680 km^2) (Figure 3). The model was divided into individual cells with lengths and widths of 1500 ft by 1500 ft (500 m by 500 m) and an average thickness of 18 ft (5.5 m). The structural framework model included overburden from ground level and encompassed 12 zones (Table 1). On average, the model had a gross thickness of 5550 ft (1692 m); Table 1 contains individual model zone thicknesses. The cell thickness averaged 5.5 ft (1.7 m) in the reservoir sections and 18.8 ft (5.7 m) for the interburden and confining zones. The final geologic model grid was approximately 6.2 million cells.

Table 1. Geologic Model Zonation with Number of Layers, Average Cell Heights, and Average Zone thicknesses

Model Zone	Number of Layers	Average Cell Height, ft (m)	Average Zone Thickness, ft (m)
Ground Surface to Hell Creek	25	31.2 (9.5)	780 (237.7)
Hell Creek	10	28.1 (8.6)	281 (85.6)
Fox Hills	10	29.9 (9.1)	299 (91.1)
Pierre	80	24.3 (7.4)	1947 (593.4)
Greenhorn	15	24.8 (7.6)	373 (113.7)
Mowry	4	21 (6.4)	84 (25.6)
Skull Creek	10	24.1 (7.3)	241 (73.5)
Inyan Kara	30	7.4 (2.3)	222 (67.7)
Swift	30	24.8 (7.6)	744 (226.8)
Piper–Picard	12	11.9 (3.6)	143 (43.6)
Opeche	6	13 (4)	78 (23.8)
Broom Creek	70	3.7 (1.1)	261 (79.6)
Amsden	5	20 (6.1)	100 (30.5)

Petrophysical log analyses for multiple wells were used to approximate the porosity (i.e., total and effective) and permeability for the geologic model. Well log data (e.g., porosity, permeability, and lithology) were averaged to upscale the data to the cells of the structured grid in preparation for property modeling. Variograms were developed to establish the spatial and vertical correlation of the model properties; however, given the sparse well control, variogram parameters could not confidently be inferred. Therefore, generic variograms were developed based on available literature and the depositional setting and paleogeography of each reservoir. The generic variogram ranges selected were 10,000 ft (3048 m) in both the major and minor axis and 10 ft (3.048 m) in the vertical direction for all zones.

Lithofacies distributions for the model consisted of shale, siltstone, fine sandstone, sandstone, dolomitic sandstone, dolostone, and anhydrite. The lithofacies for reservoir zones were distributed using the sequential indicator simulation algorithm in Petrel. The upper confining Skull Creek zone was modeled as shale, while the lower Amsden was modeled as dolostone. The interburden (Swift, Piper–Picard, and Opeche Formations) consisted of shale and siltstone. The secondary confining zone (Pierre, Greenhorn, and Mowry Formations) above the Inyan Kara was modeled as shale. The Inyan Kara reservoir is primarily fine sandstone (55%) and shale (45%). The Broom Creek reservoir was characterized by higher heterogeneity and consisted of sandstone (45%), dolomitic sandstone (14%), dolostone (34%), and anhydrite (7%).

Effective porosity from upscaled cells and established horizontal and vertical variograms were used to populate the petrophysical property volume using the Gaussian random function algorithm in Petrel. Permeability upscaled cells, established horizontal and vertical variograms, and the previously distributed effective porosity property were used to distribute permeability using the Gaussian random function algorithm. Table 2 provides a summary of modeled porosity and permeabilities by zone.

Other modeled properties included temperature and pressure, and both were distributed across the model using regional gradients. The Inyan Kara was projected to average 125°F (51.7°C) in the model, with the Broom Creek averaging 137°F (58.3°C). The average pressure of the Inyan Kara reservoir was 1863 psi (12.8 MPa), with an average of 2455 psi (16.9 MPa) for the Broom Creek reservoir.

Table 2. Petrophysical Property Statistics of the Modeled Inyan Kara and Broom Creek Formations

Geologic Properties		
Formation	**Property**	**Property Mean (range)**
Skull Creek	Effective Porosity, %	0.005 (0–24)[1]
	Permeability, mD	0.004 ($8.4E^{-07}$–0.063)[2]
Inyan Kara	Effective Porosity, %	15.1 (0–34)[1]
	Permeability, mD	3.69 ($8.4E^{-07}$–1185)[2]
Interburden	Effective Porosity, %	3.0 (0–22)[1]
	Permeability, mD	0.0063($2.5E^{-07}$–0.99)[2]
Broom Creek	Effective Porosity, %	13.3 (0–42)[1]
	Permeability, mD	5.04 ($5E^{-09}$–3440)[2]

[1] Porosity values are reported as the arithmetic mean followed by the range of values in parentheses.
[2] Permeability values are reported as the geometric mean followed by the range of values in parentheses.

Dynamic Numerical Simulation Scenarios

The numerical simulation model focused on the stacked Inyan Kara and Broom Creek Formations, which were modeled with open lateral boundary conditions. The Peng–Robinson equation-of-state (EOS) model (Peng and Robinson, 1976) was used in the simulation fluid model. Computer Modelling Group's (CMG's) WinProp was used to generate the EOS-tuned fluid model (Computer Modelling Group, 2021b). CMG uses EOS parameters to estimate fluid properties such as density, viscosity, and CO_2 solubility at reservoir temperature and pressure conditions (Nghiem and others, 2009). Representative relative permeability curves based on basin knowledge were assigned to model grid blocks for the lithofacies in each formation. CMG's GEM simulator was used to simulate injection scenarios, as described below (Computer Modelling Group, 2021a).

Separate vertical injection wells (4.5"/0.114-m tubing) were placed at the Well B location for the Inyan Kara and Broom Creek Formations. The CO_2 injection rates for each well in the simulation model were controlled by a maximum wellhead pressure (WHP) and bottomhole pressure (BHP) constraint. In accordance with U.S. Environmental Protection Agency underground injection control guidelines, the maximum BHP used in the simulation was set to not exceed 90% of a typical fracture propagation pressure known for the injection zones in the modeled area (U.S. Environmental Protection Agency, 2018), which are approximately 2300 psi (15.9 MPa) and 3100 psi (21.4 MPa) for the Inyan Kara and Broom Creek, respectively. For the WHPs, 1200 psi (8.3 MPa) and 1700 psi (11.7 MPa) were used as the surface injection pressures for the given injection tubing size used and respective depths of the Inyan Kara and Broom Creek Formations. The injectivity of CO_2 in each well was influenced by the property distributions within the geologic model, BHP constraints, and WHP maximums. Three injection scenarios were simulated:

- Stand-alone Inyan Kara injection
- Stand-alone Broom Creek Injection
- Simultaneous Inyan Kara and Broom Creek injection with two separate wells

The cumulative CO_2 injection with a stand-alone injection well in the Inyan Kara Formation was 14 million tonnes at the end of 20 years. The Broom Creek Formation accepted 22 million tonnes with a stand-alone injection well at the end of 20 years. Given the set input parameters and limits, the simultaneous injection into both formations resulted in simulated cumulative injection volumes of CO_2 that were identical to the stand-alone cases: 14 million tonnes in the Inyan Kara Formation and 22 million tonnes in the Broom Creek Formation at the end of 20 years. The resulting 20-year average injection rates were 0.70 million tonnes/year and 1.13 million tonnes/year for the Inyan Kara and Broom Creek Formations, respectively. The maximum increase in reservoir pressure due to CO_2 injection was approximately 635 psi (4.4 MPa) in the Inyan Kara and 523 psi (3.6 MPa) in the Broom Creek Formation. The estimated CO_2 plume size for the Inyan Kara Formation was 6190 acres (25.0 km^2) and was 6199 acres (25.1 km^2) for the Broom Creek Formation. Similar pressure buildups and footprints of CO_2 plumes were observed for the case with simultaneous injection into both formations, and no vertical hydraulic conductivity was observed.

MECHANICAL EARTH MODELING

A MEM has been used to identify in situ and dynamic stresses and pore pressure in the subsurface in response to fluid injection. During CO_2 injection into storage formations, pore pressure increases while reservoir temperature decreases. These changes of pore pressure and temperature induce localized stress variations that could cause formation integrity issues during CO_2 injection and storage. 1D MEMs are created along wellbores from well log and drilling data to identify current in situ stress conditions. Using the 1D MEMs for calibration, 3D MEMs are created for stress stability analysis and identifying potential integrity issues, such as induced seismicity from reactivating critically stressed faults in response to CO_2 injection, unintended CO_2 migration from storage intervals due to a ruptured confining zone, localized permeability changes, and other geomechanical hazards.

1D MEM

The 1D MEM process was completed using Schlumberger's TechLog Petrophysical software (Schlumberger, 2020b) and is based on constitutive property elastic theory and known mechanical property correlations. Four 1D MEMs were completed as part of this case study, and the resulting outputs are displayed in Figures 4–7 for Wells A, B, C, and D, respectively. For each well, the wellbore data were reviewed for quality control. Well log data, such as gamma ray log, density log, compressional and shear sonic logs, and resistivity logs, along with petrophysical interpretation results, provided inputs from the ground surface through zones of interest. Vertical stress (i.e., overburden, Sv) was calculated and calibrated with the density log, then used to estimate formation and confining zone pore pressure based on sonic and resistivity logs and direct pressure measurements. The vertical stress and pore pressure were then used, along with sonic logs and static lab measurements, to estimate static and dynamic elastic properties (e.g., Young's modulus and Poisson's ratio) and to model rock strength (e.g., unconfined compressive strength and internal friction angle). Using the elastic and rock strength properties, the magnitudes of minimum (Shmin) and maximum (SHmax) horizontal stress were calculated. Directions for both minimum and maximum horizontal stress were estimated with the image logs, caliper logs, and regional knowledge. The 1D MEM interpretation was then calibrated with events experienced during drilling (e.g., stuck pipe, tight spot, total losses, partial losses, inflow, gas kick, pack off, ballooning, and caving).

After the 1D MEM results were assessed, a MEM AOI was established to limit overall model size and focus on the CO_2 injection results from the three simulation cases (Figure 3). For stress calibration of the 3D MEM, Well A was used to verify regional stress patterns and was excluded from further analysis to reduce cell count for the AOI grid since it was more than 30 mi (48 km) away from injected CO_2 plumes. Well B was also excluded because of multiple severe fluid loss events during drilling and resulting high data uncertainty from poor wellbore conditions. The 1D MEMs for Well C and Well D, situated near the location selected for the injection wells, provided excellent matches with drilling events, suggesting a reliable calibration. Wells C and D also show a consistent stress trend, providing high-quality 1D MEM results to be used for calibrating the stress calculation of the 3D MEM by using the calculated overburden (Sv), maximum horizontal stress (SHmax), and minimum horizontal stress (Shmin). The 1D MEMs for these four wells conclude that the MEM AOI has the normal stress regime (i.e., Sv > SHmax > Shmin).

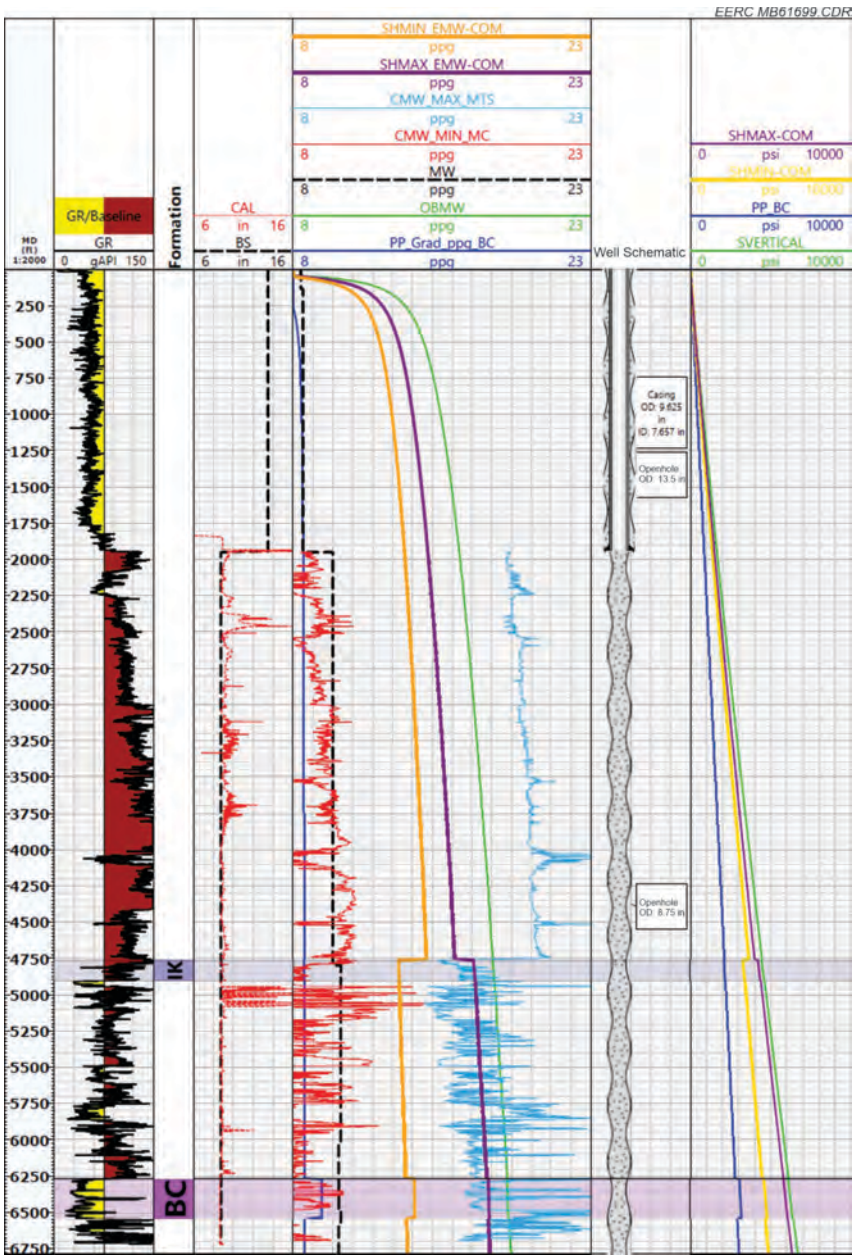

Figure 4. 1D MEM of Well A with Inyan Kara (IK) and Broom Creek (BC) indicated. Well logs displayed in tracks from left to right are 1) measured depth track (ft); 2) gamma ray log (GR); 3) caliper log (CAL) in red and bit size (BS) in black; 4) stress and pressure gradients in equivalent mud weight (EMW) (pore pressure gradient [PP_Grad] in blue, overburden mud weight gradient [OBMW] in green, maximum horizontal stress [SHMAX_EMW] in purple, minimum horizontal stress [SHMIN_EMW] in orange, breakdown pressure [CMW_MAX] in light blue, breakout pressure [CMW_MIN] in red, and mud weight [MW] in black); 5) well schematic with notes; 6) absolute stresses and pressure (pore pressure [PP] in blue, overburden [SVERTICAL] in green, maximum horizontal stress [SHMAX] in purple, and minimum horizontal stress [SHMIN] in orange). Average unconfined compressive strength (UCS in psi) and internal friction angle (FA in degree) of IK and BC: IK (5225 psi, 34.7°), BC (12,332 psi, 36.9°).

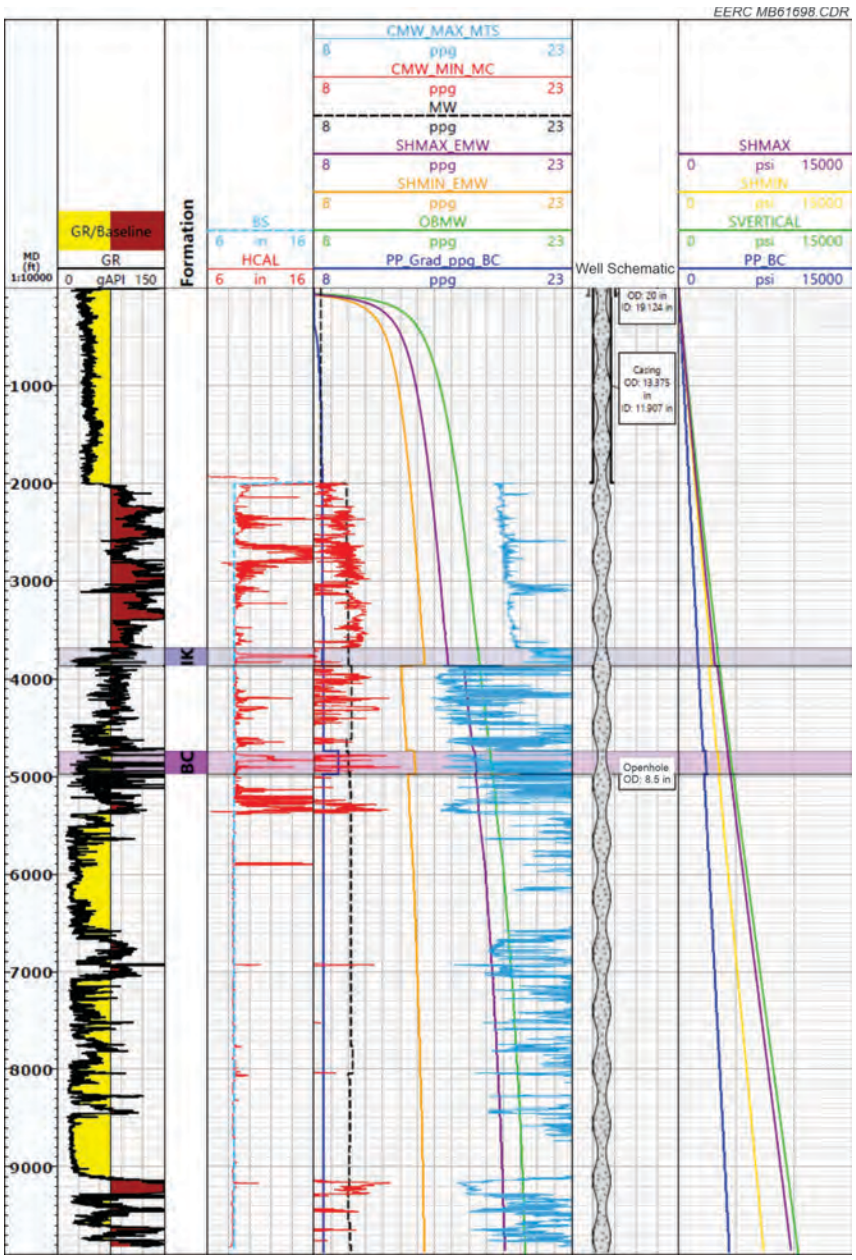

Figure 5. 1D MEM of Well B with Inyan Kara (IK) and Broom Creek (BC) indicated. Well logs displayed in tracks from left to right are 1) measured depth track (ft); 2) GR log; 3) CAL log in red and BS in black; 4) stress and pressure gradients in equivalent mud weight (EMW) (pore pressure gradient [PP_Grad] in blue, OBMW in green, maximum horizontal stress [SHMAX_EMW] in purple, minimum horizontal stress [SHMIN_EMW] in orange, breakdown pressure [CMW_MAX] in light blue, breakout pressure [CMW_MIN] in red, and MW in black); 5) well schematic with notes; 6) absolute stresses and pressure (pore pressure [PP] in blue, overburden [SVERTICAL] in green, maximum horizontal stress [SHMAX] in purple, and minimum horizontal stress [SHMIN] in orange). Average unconfined compressive strength (UCS in psi) and internal friction angle (FA in degree) of IK and BC: IK (8287 psi, 34.9°), BC (18169 psi, 39.7°).

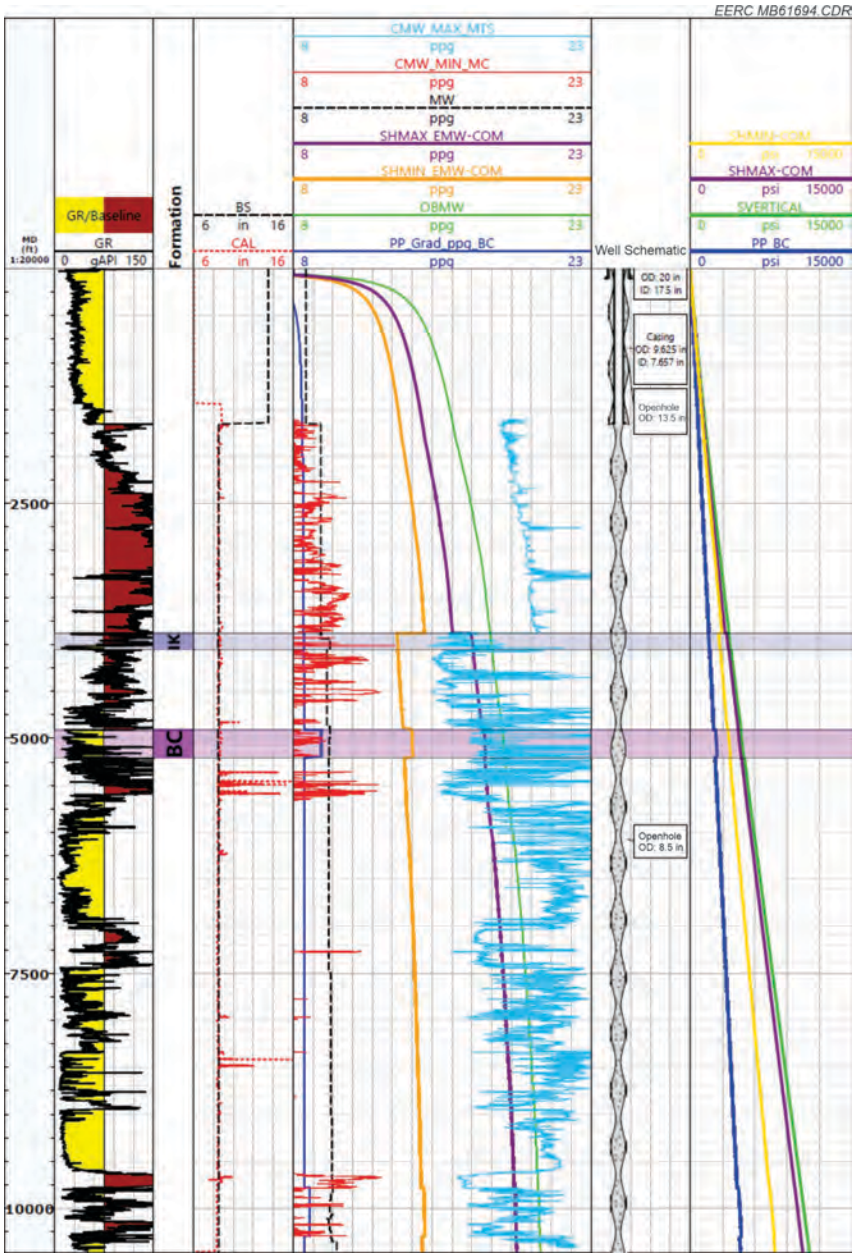

Figure 6. 1D MEM of Well C with Inyan Kara (IK) and Broom Creek (BC) indicated. Well logs displayed in tracks from left to right are 1) measured depth track (ft); 2) GR log; 3) CAL log in red and bit size (BS) in black; 4) stress and pressure gradients in equivalent mud weight (EMW) (pore pressure gradient [PP_Grad] in blue, OBMW in green, maximum horizontal stress [SHMAX_EMW] in purple, minimum horizontal stress [SHMIN_EMW] in orange, breakdown pressure [CMW_MAX] in light blue, breakout pressure [CMW_MIN] in red, and MW in black); 5) well schematic with notes; 6) absolute stresses and pressure (pore pressure [PP] in blue, overburden [SVERTICAL] in green, maximum horizontal stress [SHMAX] in purple, and minimum horizontal stress [SHMIN] in orange). Average unconfined compressive strength (UCS in psi) and internal friction angle (FA in degree) of IK and BC: IK (6896 psi, 32.8°), BC (13134 psi, 37.2°)

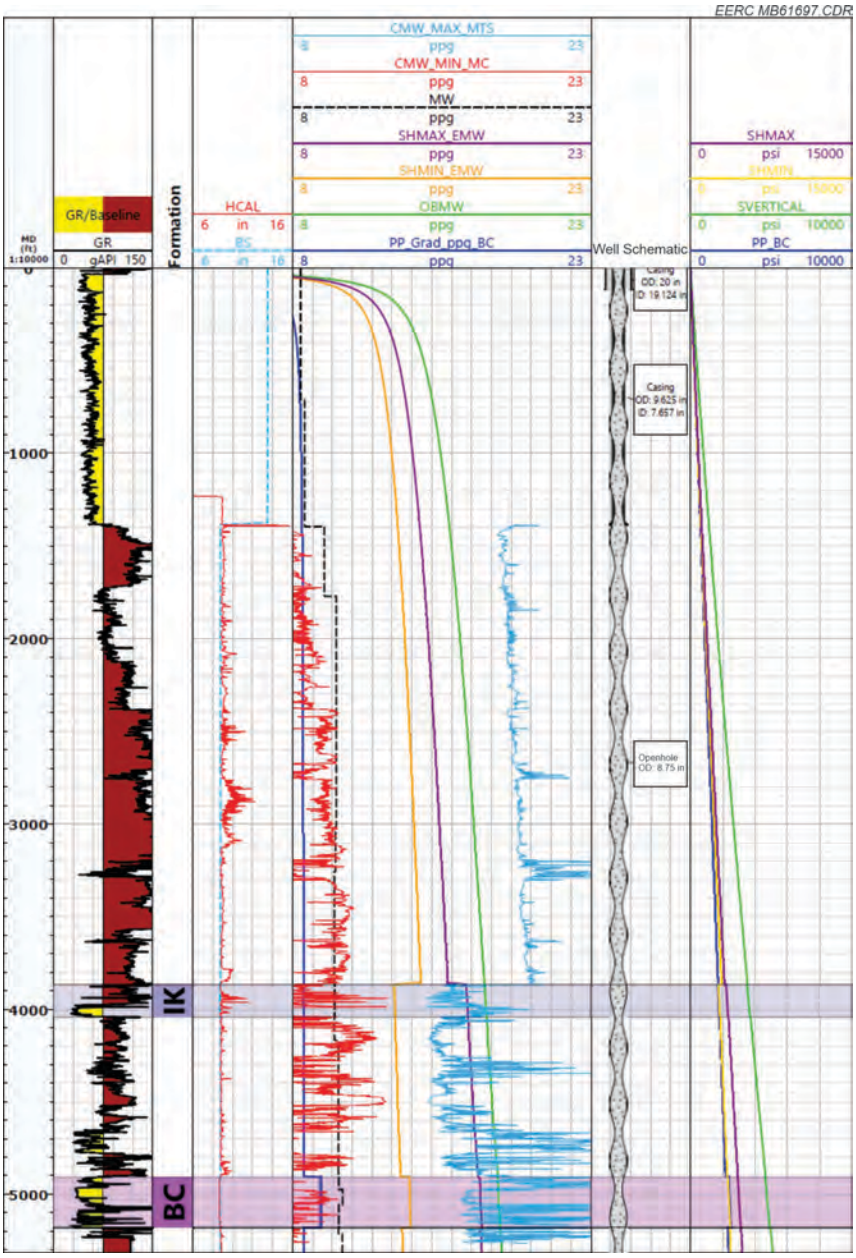

Figure 7. 1D MEM of Well D with Inyan Kara (IK) and Broom Creek (BC) indicated. Well logs displayed in tracks from left to right are 1) measured depth track (ft); 2) GR log; 3) CAL log in red and BS in black; 4) stress and pressure gradients in equivalent mud weight (EMW) (pore pressure gradient [PP_Grad] in blue, OBMW in green, maximum horizontal stress [SHMAX_EMW] in purple, minimum horizontal stress [SHMIN_EMW] in orange, breakdown pressure [CMW_MAX] in light blue, breakout pressure [CMW_MIN] in red, and MW in black); 5) well schematic with notes; 6) absolute stresses and pressure (pore pressure [PP] in blue, overburden [SVERTICAL] in green, maximum horizontal stress [SHMAX] in purple, and minimum horizontal stress [SHMIN] in orange). Average unconfined compressive strength (UCS in psi) and internal friction angle (FA in degree) of IK and BC: IK (5197 psi, 32.8°), BC (12771 psi, 37.6°).

3D MEM

With the completed 1D MEMs for Wells C and D, the following assumptions were used to create and calibrate 3D MEMs for each dynamic numerical simulation case and conduct a stress stability analysis:

- Changes to porosity and permeability due to CO_2 injection are considered negligible for basins with consolidated rock (i.e., Williston Basin) and can be ignored to allow for one-way simulation between pore pressure and stress to be used. Pore pressure is allowed to affect changes in stress, with no changes allowed in the opposite direction.

- Temperature differentials between the reservoir and injected fluids can induce thermal stress. The induced thermal stress can increase permeability. However, the area impacted by the thermal stress is limited near the injection wellbore (Jiang and others, 2017) and can be considered negligible at reservoir scale. This case study considers a one-way thermal effect and assumes the temperature change generates thermal stress without increases to permeability that can impact the overall stress evolution.

- For this experiment, wells injecting CO_2 were assumed to maintain a constant temperature (60°F [15.6°C]) at the wellbore and the far field maintains a constant initial reservoir temperature. Temperature propagation is assumed to occur by lateral heat conduction only, without vertical conduction or convection.

- Postfailure behavior (e.g., mechanical behavior after rock starts to fail or yield plasticly) is considered minor for this model, and identification of location and timing of failure occurrence was of greater importance than failure magnitude. Simulation of postfailure behavior was assumed to be currently unnecessary.

- For this iteration of the 3D MEM, natural faulting and fractures were ignored for injection layers, interburden, and confining zones.

Using these assumptions, the 3D MEM model was built with the Visage plug-in in Petrel (Schlumberger, 2020c). To model the stress equilibrium and achieve numerical stability for the AOI, additional gridded volume was added around and below the stacked storage zones of interest. To ensure unwanted boundary effects for the AOI, sideburden and underburden volume default values for Visage were used, expanding the grid volume more than 3500 times over the AOI alone (Figure 8). A tartan grid pattern was used outside the AOI for a more modest cell count increase given the extra volume. From the AOI boundary, the grid was laterally extended to about 345,000 ft (105,000 m) on each side and deepened to a depth of 371,200 ft (113,142 m). This additional cell count required the zones above the Greenhorn to be coarsened to 20 layers, with all other zones using the same layering scheme as the geologic model grid (Table 3). Within the AOI, the final grid had about 2.7 million cells (114 by 116 by 217 cells) with lengths and widths of 1000 ft by 1000 ft (305 m by 305 m). The addition of the sideburden and underburden increased the grid to 3.5 million cells (126 by 128 by 217 cells). The volumes of underburden and sideburden were intended only for numerical stability within the modeling process and have no physical meaning beyond that purpose.

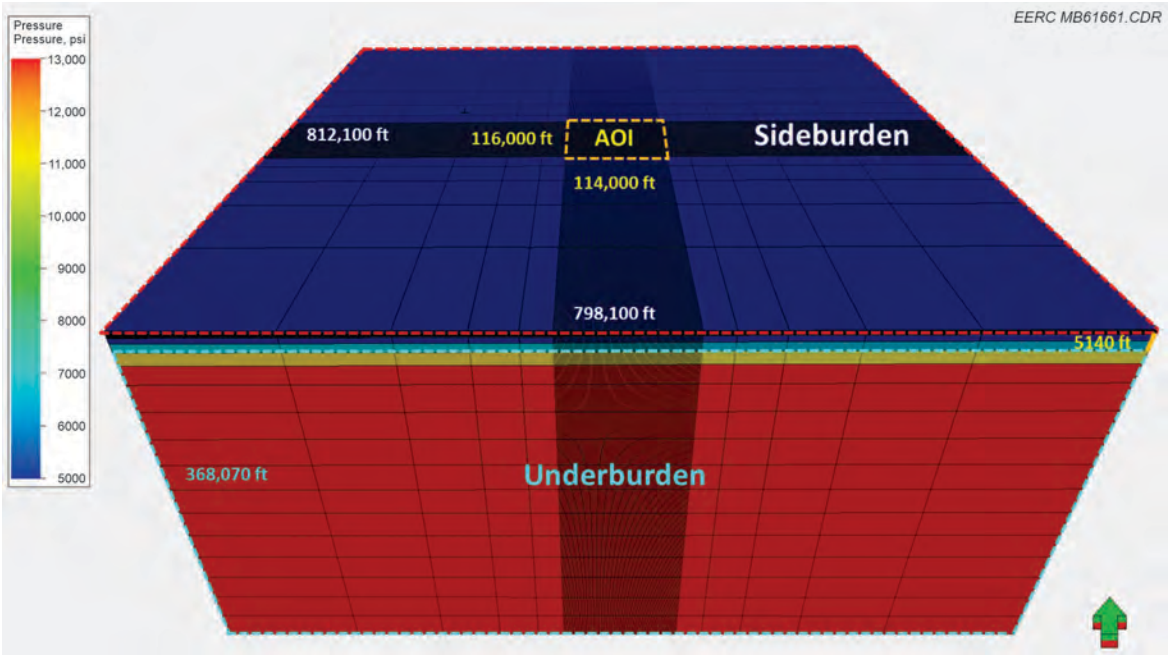

Figure 8. 3D MEM grid, with the AOI indicated with a yellow dashed line along with the additional sideburden (surrounding AOI grid) and underburden (below teal line) added to the grid for Visage simulation. Initial pore pressure (psi) displayed prior to CO_2 injection.

Table 3. 3D MEM Zonation with Number of Layers and Average Cell Heights

Model Zone	Number of Layers	Average Cell Height, ft (m)
Ground Surface to Greenhorn	20	156 (47.5)
Greenhorn	15	25 (7.6)
Mowry	4	17 (5.2)
Skull Creek	10	24 (7.3)
Inyan Kara	30	6 (1.8)
Swift	30	24 (7.3)
Piper–Picard	12	9 (2.7)
Opeche	6	9 (2.7)
Broom Creek	70	4 (1.2)
Amsden (100 ft)	5	20 (6.1)
Datum Level 77,132 ft	5	14,800 (4511)
Datum Level 371,200 ft	10	29,400 (8961)

The pore pressure for each time step of the three simulated scenarios was upscaled to the geomechanical grids: stand-alone Inyan Kara injection, stand-alone Broom Creek injection, and simultaneous Inyan Kara and Broom Creek injection. Using the 1D MEM stress results from Well C and Well D, the initial conditions of the stress state for the geomechanical grid were calibrated to best fit. By changing the 3D model boundary conditions, the simulated property volumes of Sv, SHmax, and Shmin were calibrated to the 1D MEM log results (Figure 9). The

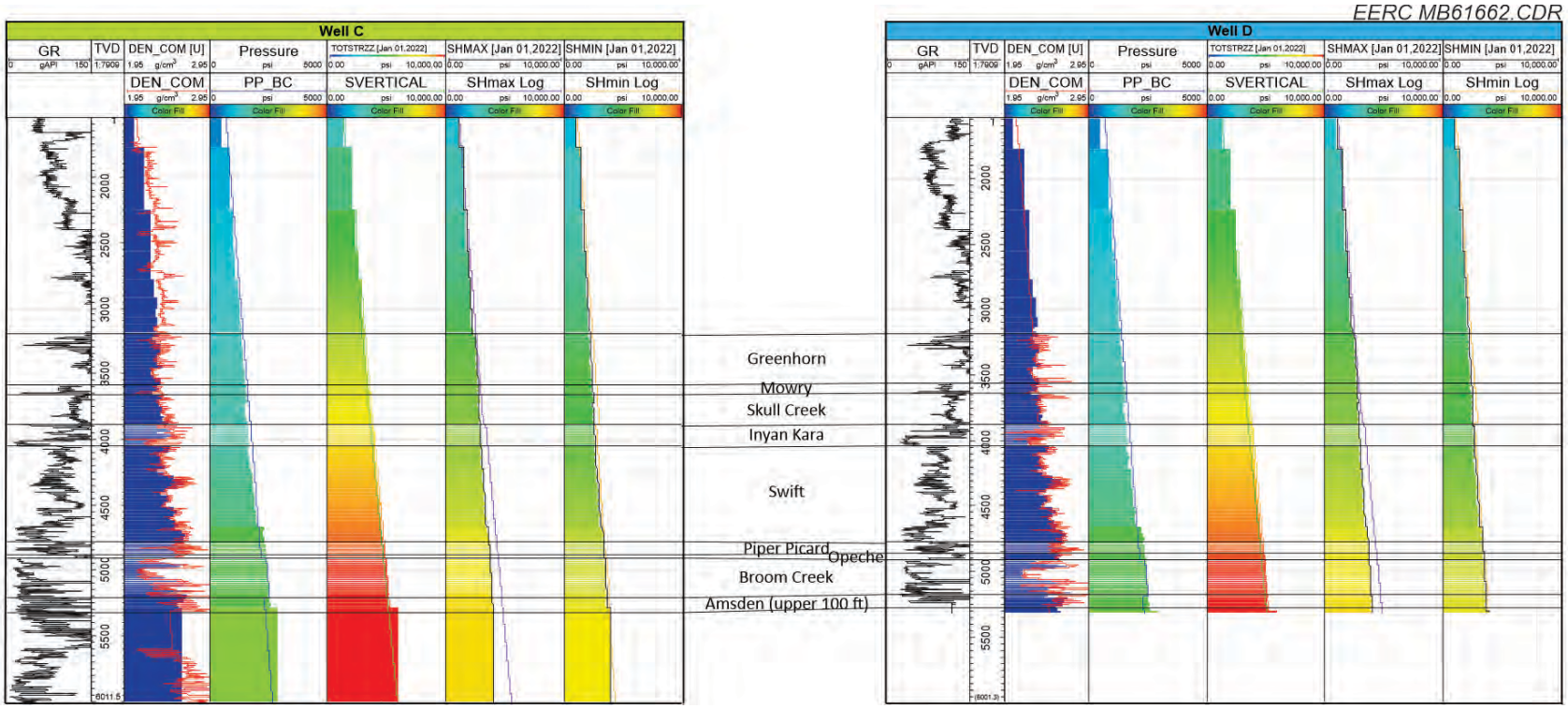

Figure 9. Comparison and calibration between 3D stress cell values and 1D MEM stress log values for Well C and Well D. Solid lines are results from the 1D MEM, and color-filled shapes show stress values for cells from the 3D MEM. Data displayed in the tracks from left to right are 1) GR in black; 2) true vertical depth (TVD) in ft; 3) density log (DEN_COM) in red and density model (DEN_COM[U]) as the color fill; 4) pore pressure log (PP_BC) in blue and pore pressure mode (Pressure) as color fill; 5) overburden log (SVERTICAL) in green and overburden model (TOTSTRZZ) as color fill; 6) maximum horizontal stress log (SHmax Log) in purple and maximum horizontal stress model (SHMAX) as color fill; and 7) minimum horizontal stress log (Shmin Log) in orange and minimum horizontal stress model (Shmin) as color fill.

stress calibration process resulted in 3D stress values within acceptable error of the 1D MEM. Sv and Shmin had errors of less than 7%, and the error for SHmax was between 10% and 20%. SHmax has a higher uncertainty as the intermediate principal stress for normal stress regimes because little to no direct calibration data are available. SHmax results and error are acceptable as they are bound by the highly calibrated Sv and Shmin.

After the CO_2 injection scenarios were simulated in Visage, Python (2021) scripts were used to postprocess results for further analysis of stress stability and identify instances of failure, temperature distribution, and thermal stress events. In the postprocessing, the Python scripts identified instances of failure using the Mohr–Coulomb failure theory (Fjaer and others, 2008) for every pore pressure time step of each scenario. The scripts used analytical solutions to calculate the temperature distribution (Equation 1) and thermal stress (Equation 2) for each time step. The temperature distributions (T[r,t]) at a point and a certain time are calculated as follows:

$$T(r,t) = T_s + (T_i - T_s)\,\mathrm{erf}\left(\frac{r}{2\sqrt{\alpha t}}\right) \quad \text{[Eq. 1]}$$

where r is the distance from the wellbore, t is the injection time, T_s is temperature at the injection wellbore (i.e., T[0,t]), T_i is initial reservoir temperature (i.e., T[r,0]), α is the thermal diffusivity (this study uses an average rock value, 1.15 mm^2/s) and erf() is the error function (Bergman and others, 2017).

The thermal stress (S_{ij}) is calculated as follows:

$$S_{ij} = \frac{E}{1-2\nu}\alpha_T(T - T_i)\delta_{ij} \quad \text{[Eq. 2]}$$

where E is Young's modulus, ν is Poisson's ratio, T is the current temperature at a point, T_i is the initial temperature at a point, α_T is the coefficient of linear thermal expansion, and δ_{ij} is the Kronecker delta (Fjaer and others, 2008). The results for each scenario and time step were loaded into Petrel for visualization, creating volumes for failure mode classification, thermal stress magnitude, shear failure indication, temperature value, and tensile failure indication.

The effective minimum horizontal stress (Shmin_e) that results from the 3D MEMs provides a summary of the stress evolution during CO_2 injection and stress stability analysis for all three simulation cases. Effective stress (σ_e) is the actual loading (stress) applied on a rock matrix (Figure 10) and is a critical component in stress stability analysis, calculated as follows:

$$\sigma_e = \sigma_t - \alpha P_0 \quad \text{[Eq. 3]}$$

where σ_t is total stress, α is Biot coefficient, and P_0 is pore pressure (Aadnøy and Looyeh, 2019). Biot coefficient is usually assumed to be 1.0 in most settings.

For rock stress stability analysis, the Mohr–Coulomb yield theory is commonly used (Figure 11). Stress at any point in 3D space can be expressed as a Mohr's circle when plotted in effective normal and shear stress space. Whenever the Mohr's circle intersects failure or yield lines (e.g., tensile failure, shear failure and compaction failure), it indicates stress conditions will cause the rock to start failing or yielding at that point. This is a very useful tool to identify failure occurrence or conditions (Dusseault, 2019).

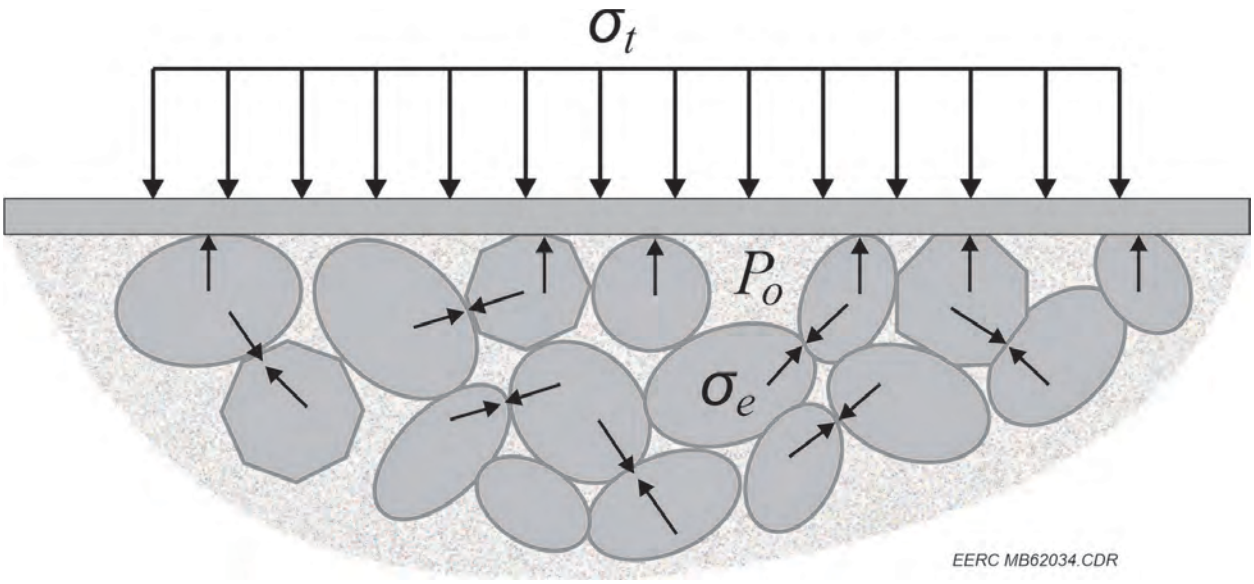

Figure 10. The concept of effective stress (σ_e) in terms of total stress (σ_t) and pore pressure (P_o) (modified after Aadnøy and Looyeh [2019]).

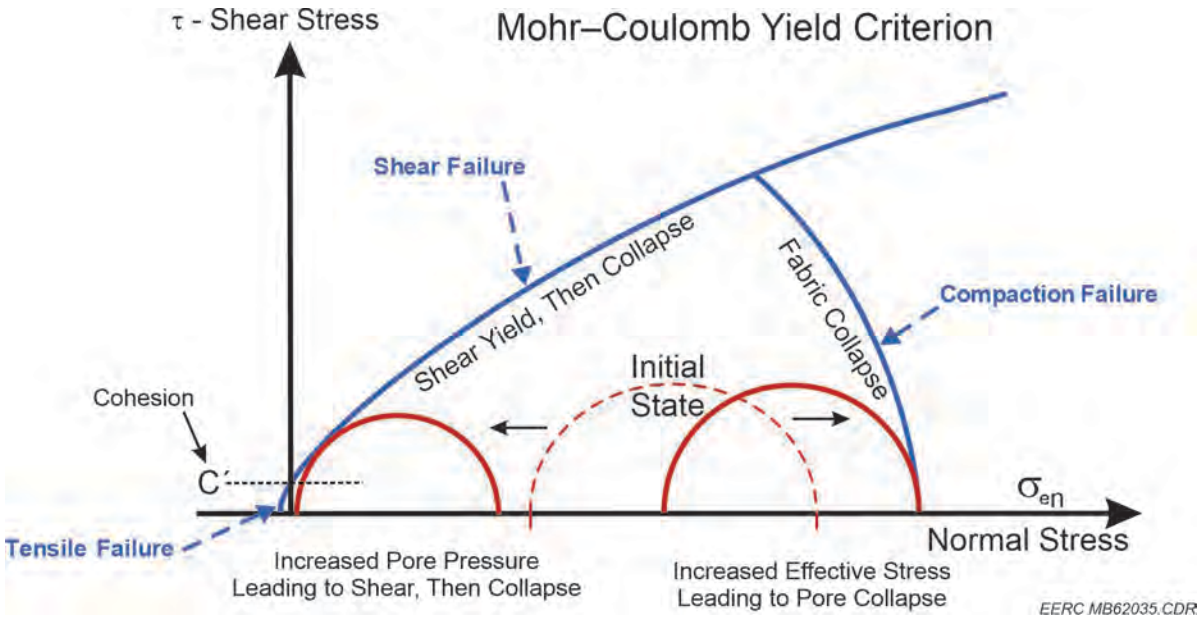

Figure 11. Graphical overview of Mohr–Coulomb yield criterion: effective normal stress (σ_{en}) and shear stress (τ). Failure lines are represented in blue and Mohr's circles are represented in red (modified after Dusseault [2019]).

Shmin_e best represents stress evolution for the normal stress regime (i.e., Sv > SHmax > Shmin) for this AOI. As pore pressure increases (i.e., CO_2 injection), Shmin_e is reduced (as

expected), resulting in a negative change when comparing difference between Shmin_e at the 20-year time step and initial Shmin_e.

The initial Shmin_e for the 3D MEMs demonstrates vertical heterogeneity based on properties and depths from the geologic model and calibrated 1D MEM stress gradients (Figure 12). Higher pore pressure gradients in the Inyan Kara and Broom Creek contribute to lower Shmin_e compared to the interburden and uppermost seal. The lower Shmin gradient shift at the top of the Inyan Kara in the 1D MEMs also contributes to the lower initial Shmin_e beneath the Skull Creek Formation.

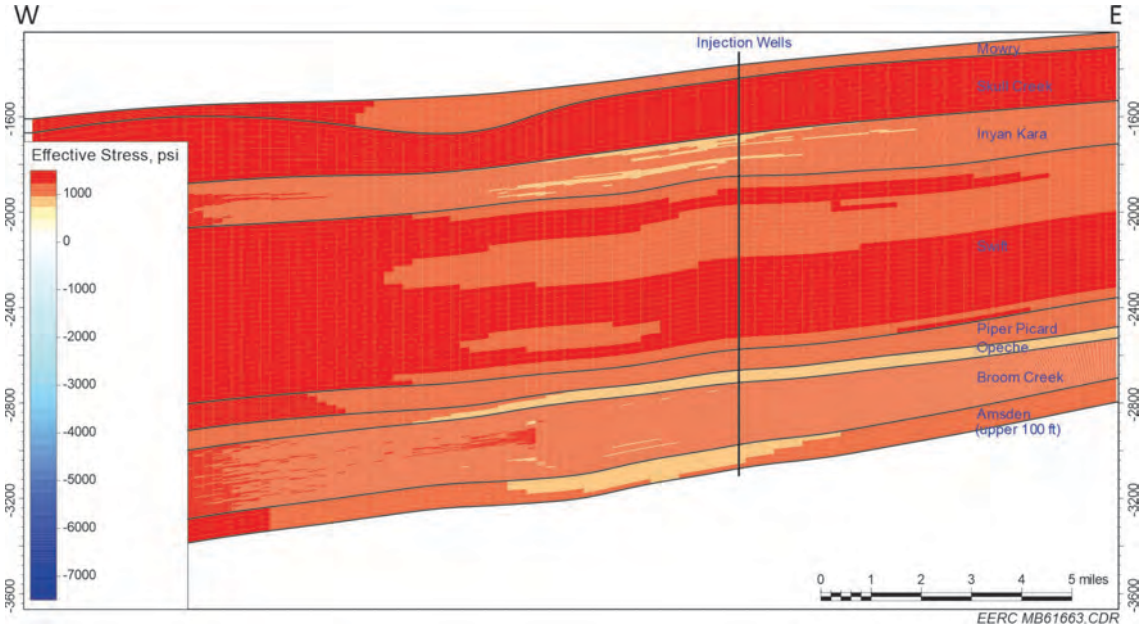

Figure 12. West-to-east cross section of the initial effective minimum horizontal stress for the 3D MEM after stress calibration. The Mowry Formation through the upper part of the Amsden Formation is displayed. Vertical scale is in feet below sea level.

Comparing the initial Shmin_e states near the injection wells to the resulting Shmin_e without thermal stress for stand-alone Inyan Kara Formation, stand-alone Broom Creek Formation, and simultaneous Inyan Kara and Broom Creek (Figures 13–15, respectively) demonstrates that the Inyan Kara and Broom Creek are geomechanically isolated by the Swift Formation. No pressure communication was found across the interburden during the injection period, and the Skull Creek Formation, the uppermost confining zone above the Inyan Kara, also showed no geomechanical failure or pressure communication to formations above. Shmin_e for each case was affected by stress changes induced by pore pressure increases over a 20-year period. The magnitude of change to Shmin_e was greatest at the injection wells, with the impacts propagating away from the injection sites associated with pore pressure change.

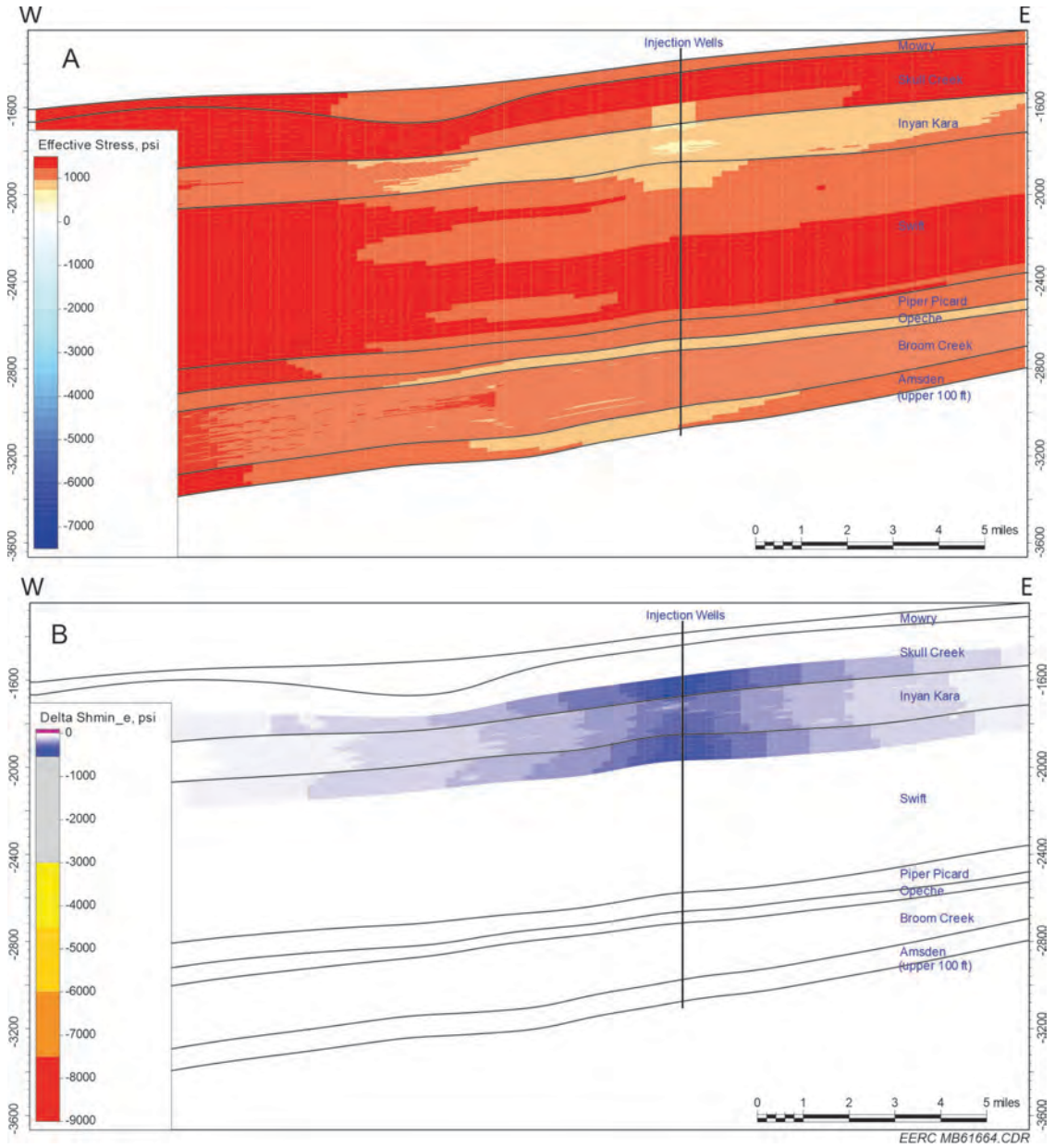

Figure 13. Effective minimum horizontal stress results without thermal stress after 20 years of CO_2 injection into the Inyan Kara Formation: A) west-to-east cross section displaying the resulting effective minimum stress magnitude and B) west-to-east cross section displaying the change in effective minimum stress from initial conditions. Vertical scale is in feet below sea level.

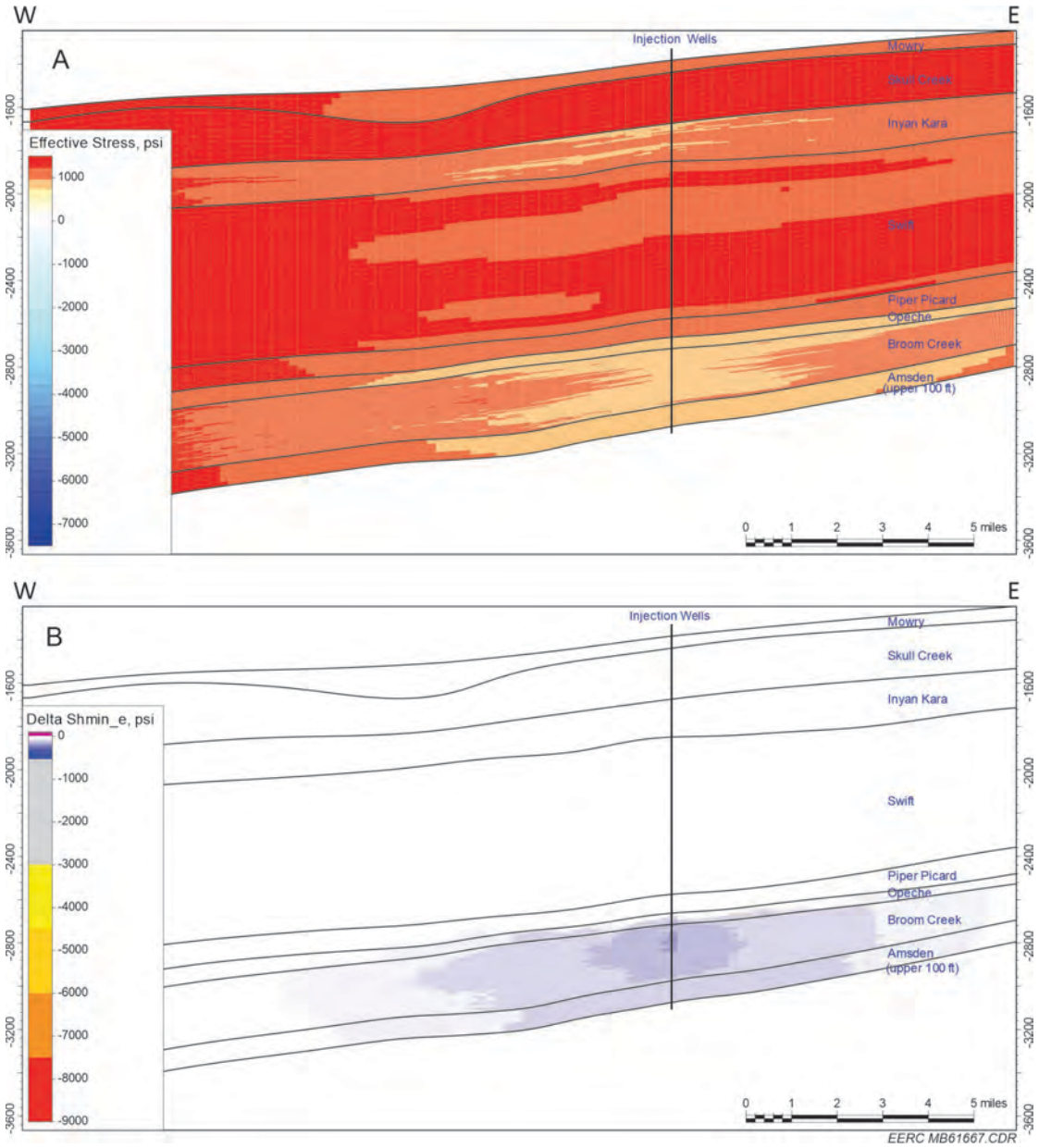

Figure 14. Effective minimum horizontal stress results without thermal stress after 20 years of CO_2 injection into the Broom Creek Formation: A) west-to-east cross section displaying the resulting effective minimum stress magnitude and B) west-to-east cross section displaying the change in effective minimum stress from initial conditions. Vertical scale is in feet below sea level.

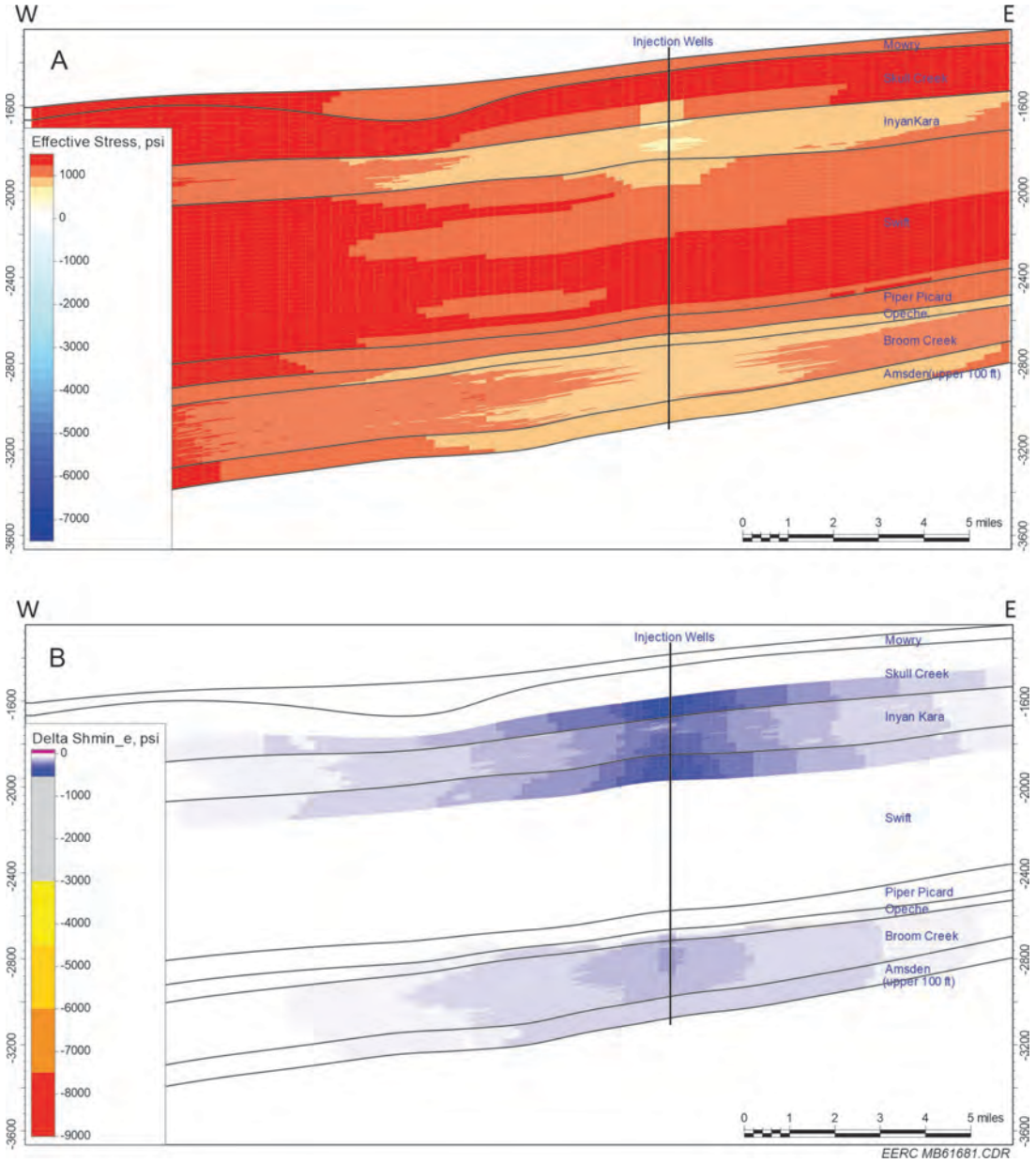

Figure 15. Effective minimum horizontal stress results without thermal stress after 20 years of CO_2 injection into the Inyan Kara and Broom Creek Formations: A) west-to-east cross section displaying the resulting effective minimum stress magnitude and B) west-to-east cross section displaying the change in effective minimum stress from initial conditions. Vertical scale is in feet below sea level.

The predicted Mohr–Coulomb failure mode classification after 20 years of CO_2 injection for the stand-alone Inyan Kara, stand-alone Broom Creek, and simultaneous Inyan Kara and Broom Creek cases (Figures 16–18, respectively) indicates the locations and types of failures to occur for the conditions. The different classifications are found at the end of injection for all cases: stability, only shear failure, only tensile failure, and both shear and tensile failure. All observed cells experiencing an identified failure mode are adjacent to the injection wells and only if thermal stress is considered for the case. Excluding thermal stress, the change of effective stress by pore pressure alone is not enough to cause any failure conditions.

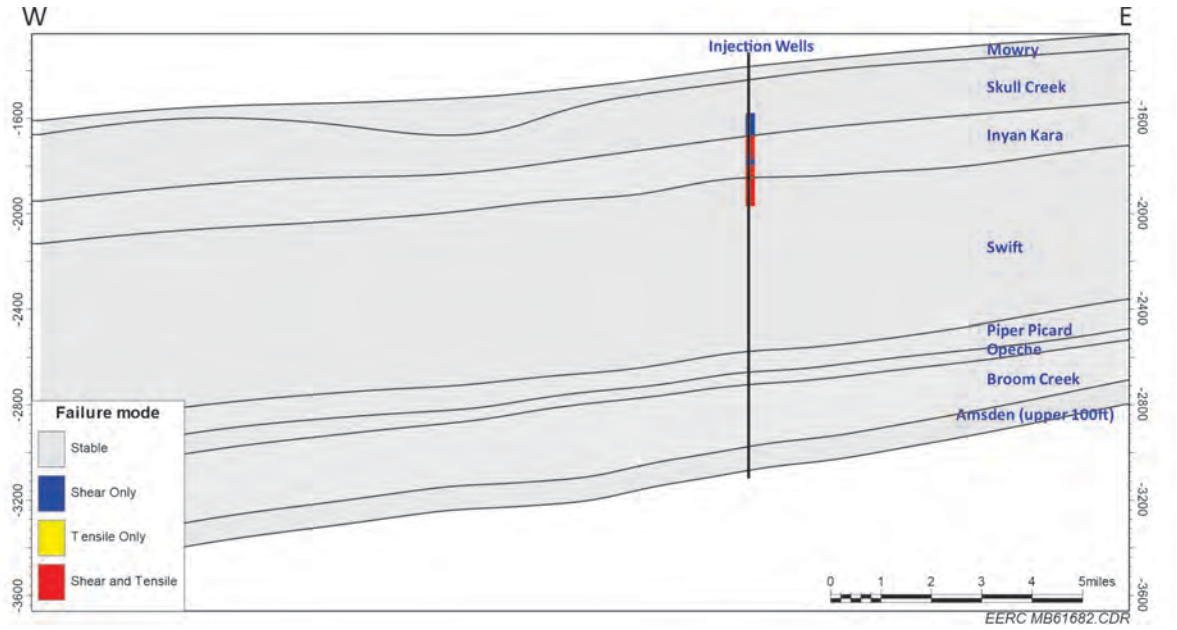

Figure 16. West-to-east cross section of the Mohr–Coulomb failure mode classification predicted after 20 years of CO_2 injection into the stand-alone Inyan Kara Formation case. Failure mode conditions are only predicted adjacent to the injection wellbore into the Inyan Kara and surrounding confining zones as shear only and shear and tensile modes. Vertical scale is in feet below sea level.

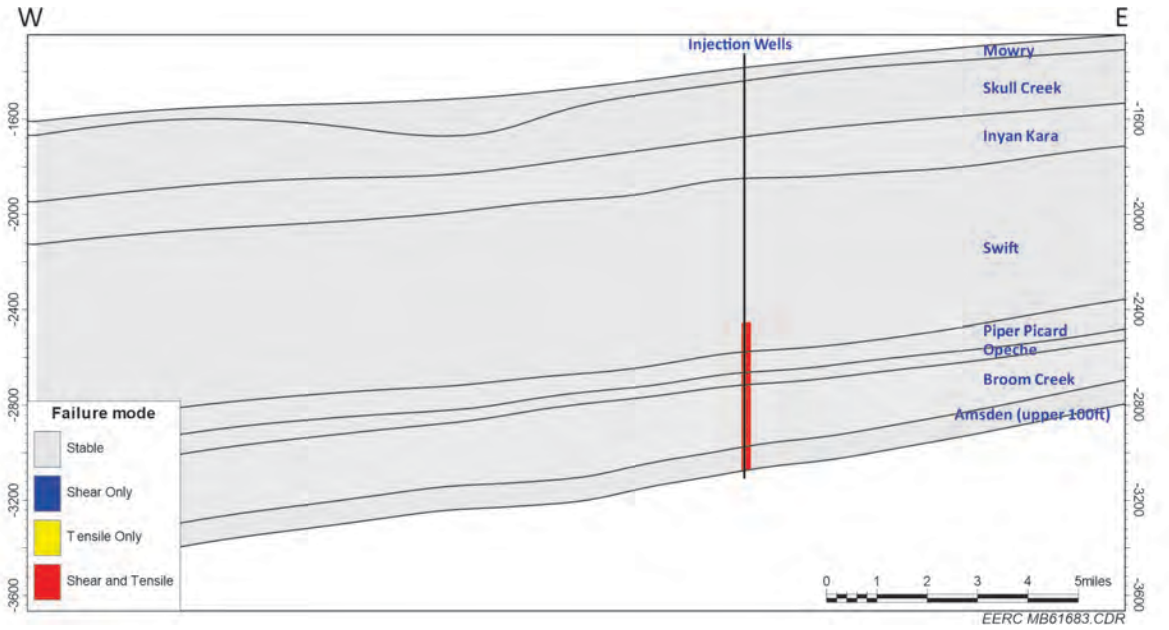

Figure 17. West-to-east cross section of the Mohr–Coulomb failure mode classification predicted after 20 years of CO_2 injection into the stand-alone Broom Creek Formation case. Failure mode conditions are only predicted adjacent to the injection wellbore into the Broom Creek and surrounding confining zones as shear and tensile modes. Vertical scale is in feet below sea level.

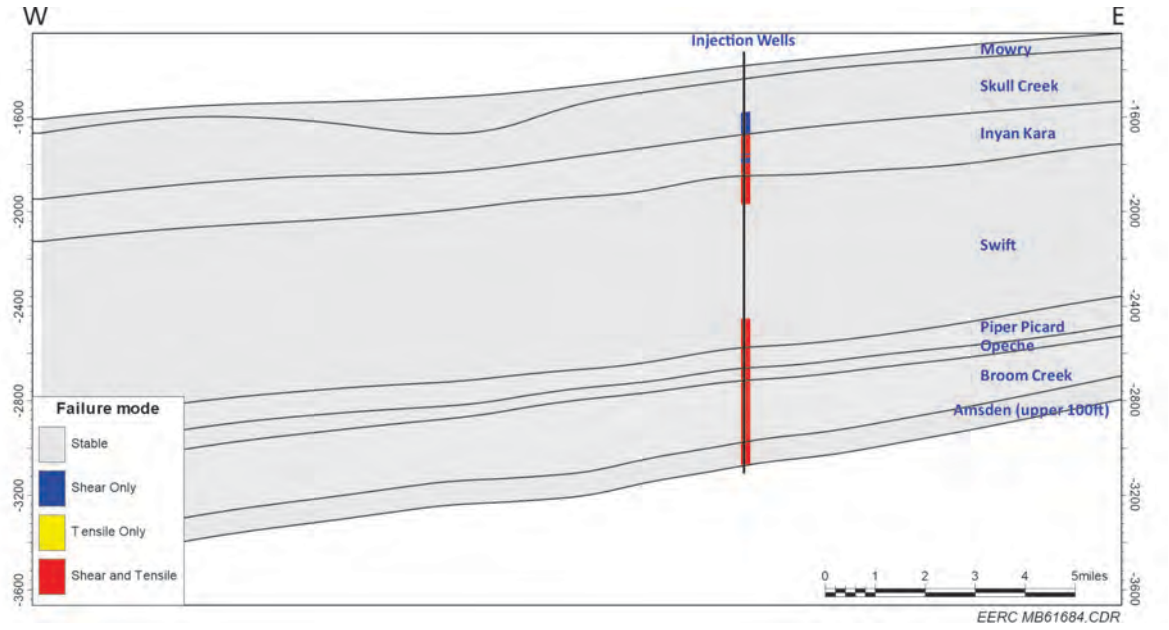

Figure 18. West-to-east cross section of the Mohr–Coulomb failure mode classification predicted after 20 years of CO_2 injection into the Inyan Kara and Broom Creek Formations simultaneously as a stacked storage scenario. Failure mode conditions are only predicted adjacent to the injection wellbore into the reservoirs and surrounding confining zones as shear only and shear and tensile modes. Vertical scale is in feet below sea level.

Identified Mohr–Coulomb failure modes are constrained to the pillar of cells containing the injection wells and are observed in the reservoir and confining zones immediately adjacent to cells receiving CO_2. No failure modes are observed to extend completely through the upper confining zone (i.e., cap rock) or interburden layers. The failure mode results are aligned with observations from the effective minimum horizontal stress discussed earlier. The current 3D MEM iteration does not consider faulting or natural fractures. The risk of reactivating critically stressed faults or natural fractures located around injection wellbores should be considered in future iterations of geomechanical analyses.

Thermal stress is generated over the 20-year CO_2 injection process from the temperature differential between the reservoirs and the injected fluid and was calculated for the stand-alone Inyan Kara, stand-alone Broom Creek, and simultaneous Inyan Kara and Broom Creek cases (Figures 19–21, respectively). Shmin_e conditions including thermal stress are compared with the initial Shmin_e conditions for the stand-alone Inyan Kara Formation, stand-alone Broom Creek Formation, and simultaneous Inyan Kara and Broom Creek (Figures 22–24, respectively). They show very similar Shmin_e evolution pattern to the cases without thermal stress, except for high-magnitude thermal stress values near the injection wellbores. The thermal stress for the simultaneous Inyan Kara and Broom Creek case behaves similarly to the stand-alone cases with independent injections into the reservoirs. The thermal stress results are constrained to the cells intersected by the injection wells. After the 20-year injection period, the thermal stress does not propagate past the cells adjacent to the injection wells. This observation suggests that the assumption of only using lateral heat conduction for the 3D MEM may be too simple or the thermal diffusivity value (α in Equation 1) is not great enough for the temperature profile to reach past the 1000-ft by 1000-ft (305-m by 305-m) cell laterally. The lack of permeability changes over the 20-year period due to thermal stress could also be underestimating the spread of thermal stress. Future investigations should consider local grid refinements adjacent to the injection wells to better estimate thermal stress propagation profiles away from the injection wells.

For all three cases, the thermal stresses generated during the injection period are mostly constrained in the injection layers. The upper confining zone and most of the interburden between the injection layers have no observed thermal stress change over the 20-year injection period. Thermal stress can be critical to overall stress stability and modify permeability during the injection. Also, critically stressed natural fractures could reactivate because of thermal stress changes during CO_2 injection, and additional sensitivities should be considered for future investigations.

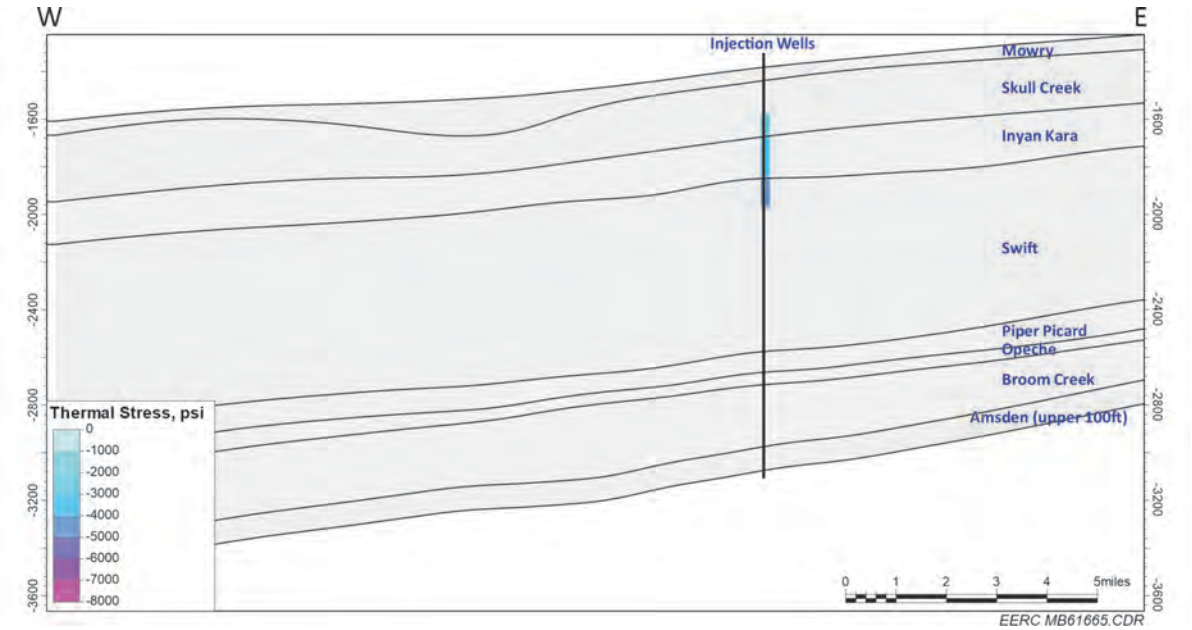

Figure 19. Thermal stress evolution for Inyan Kara after 20 years of injection. Vertical scale is in feet below sea level.

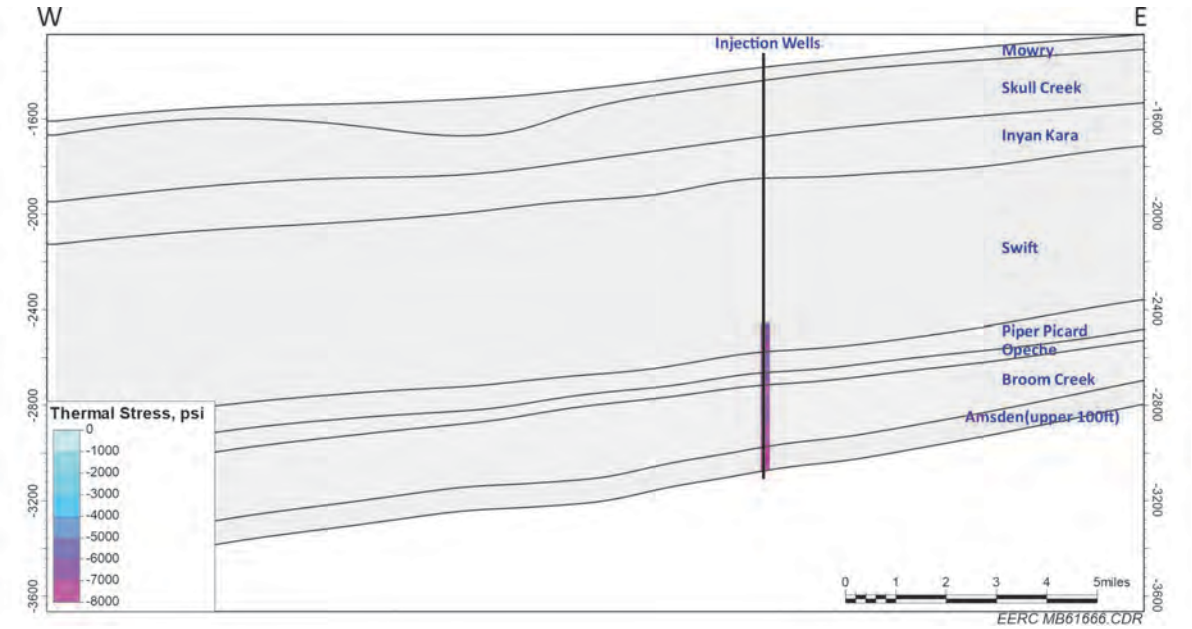

Figure 20. Thermal stress evolution for Broom Creek after 20 years of injection. Vertical scale is in feet below sea level.

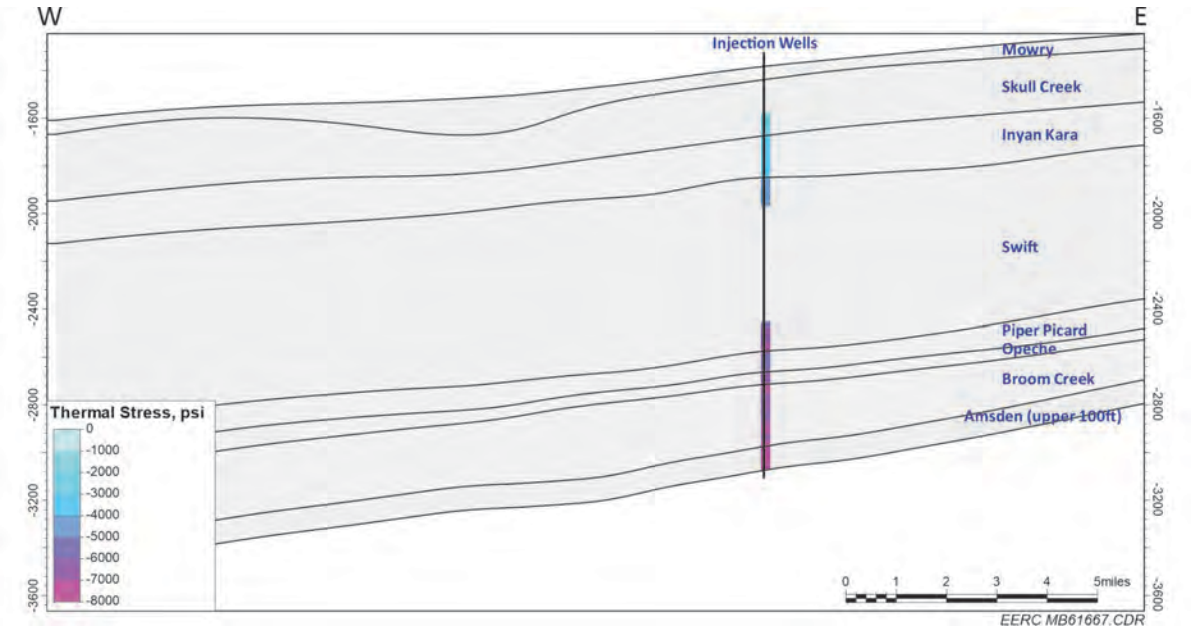

Figure 21. Thermal stress evolution for Inyan Kara and Broom Creek as stacked storage after 20 years of injection. Vertical scale is in feet below sea level.

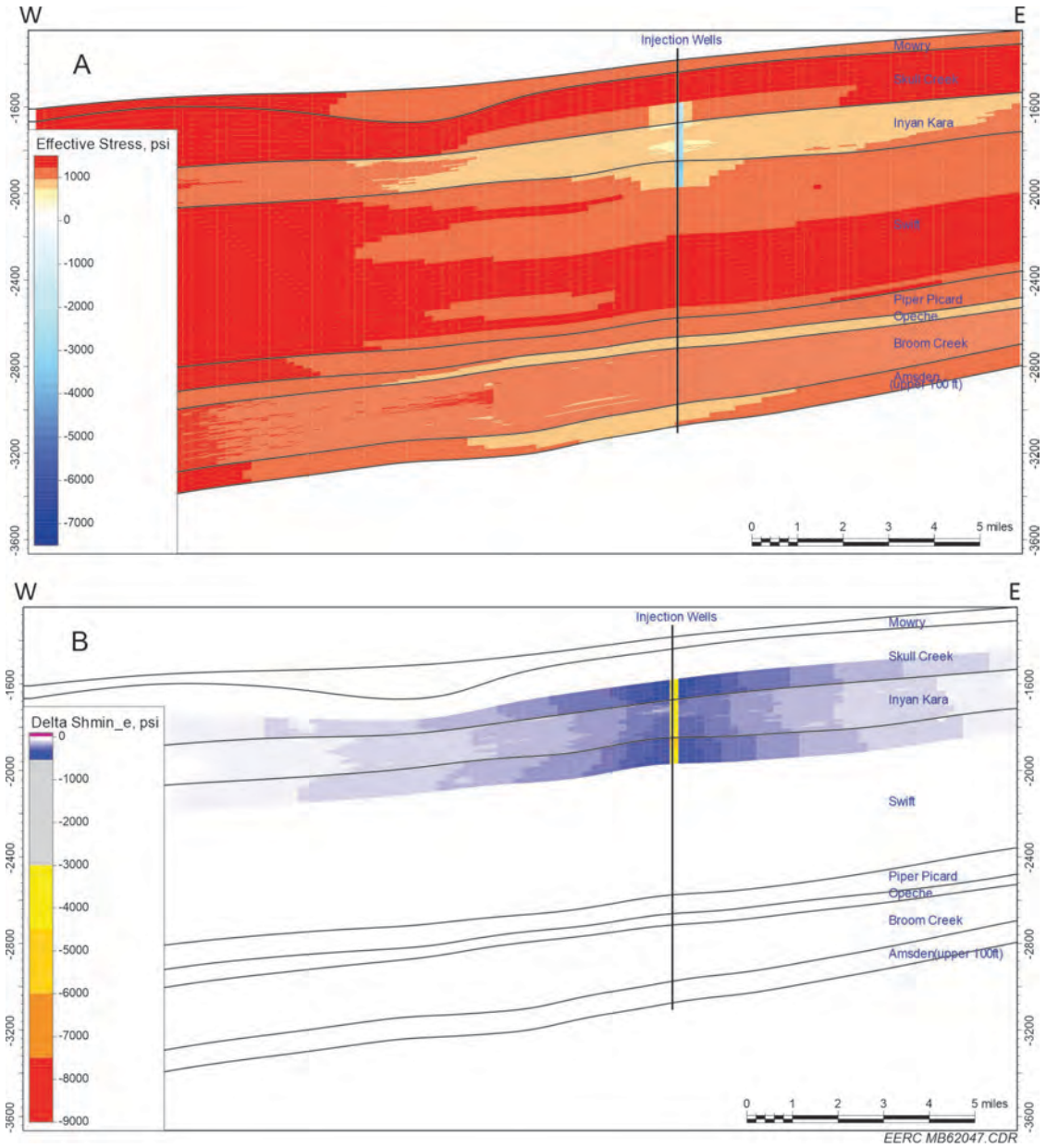

Figure 22. Effective minimum horizontal stress including thermal stress evolution results after 20 years of CO_2 injection into the Inyan Kara Formation: A) west-to-east cross section displaying the resulting effective minimum stress magnitude and B) west-to-east cross section displaying the change in effective minimum stress from initial conditions. Vertical scale is in feet below sea level.

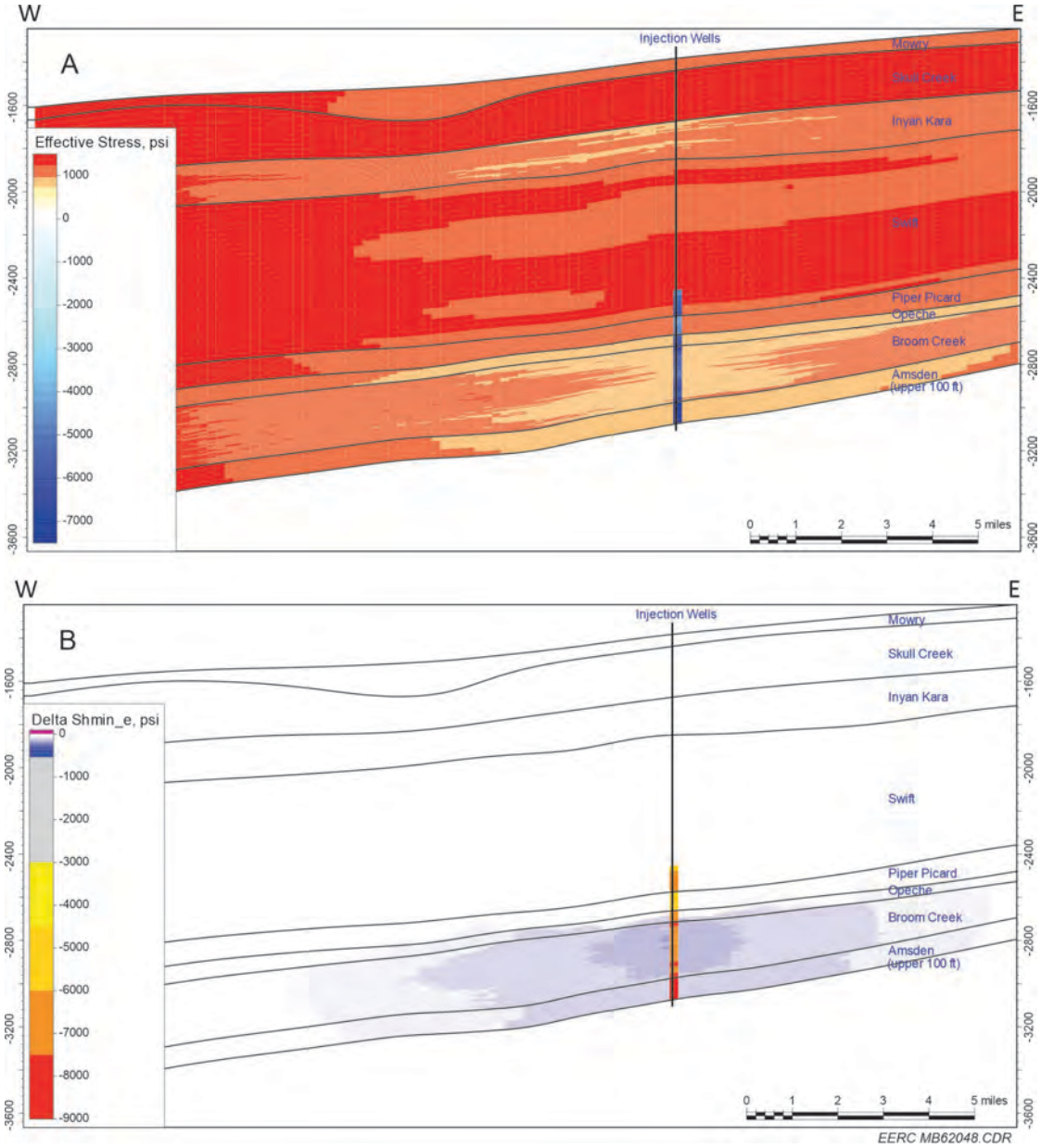

Figure 23. Effective minimum horizontal stress including thermal stress evolution results after 20 years of CO_2 injection into the Broom Creek Formation: A) west-to-east cross section displaying the resulting effective minimum stress magnitude and B) west-to-east cross section displaying the change in effective minimum stress from initial conditions. Vertical scale is in feet below sea level.

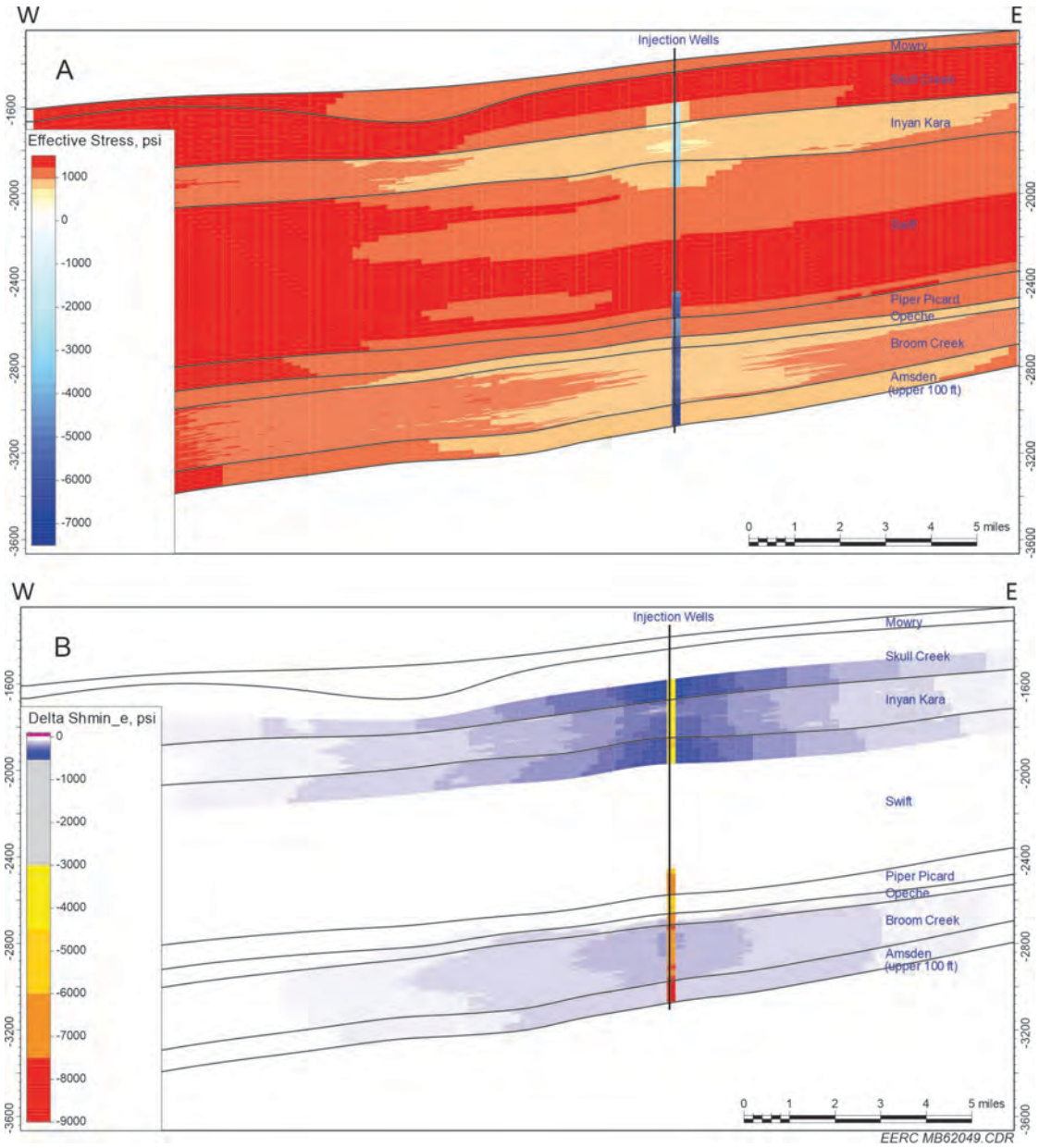

Figure 24. Effective minimum horizontal stress including thermal stress evolution results after 20 years of CO_2 injection into the Inyan Kara and Broom Creek Formations: A) west-to-east cross section displaying the resulting effective minimum stress magnitude and B) west-to-east cross section displaying the change in effective minimum stress from initial conditions. Vertical scale is in feet below sea level.

DISCUSSION AND KEY LEARNINGS

The implemented geomechanics workflow can assess the integrity and potential failure modes of the interburden and uppermost top seal for any given stacked storage scenario, provided 1) static geologic modeling is complete for the stratigraphic section from the ground surface to below the lowermost reservoir; 2) dynamic numerical simulations are conducted to estimate fluid flow for the entire injection period, including hydrocarbon or other fluid extraction that are prior or contemporary with injection; and 3) appropriate well log data and direct pressure measurements are collected on wells within the proposed AOI.

Compressional and shear sonic well logs along with direct pressure measurements and core data allow for good control on current stress conditions for planned injection reservoirs and drive the current understanding, but additional mini-frac data are necessary to better constrain Shmin uncertainty ranges, and it is critical to establish robust correlations between dynamic and static rock mechanics constitutive properties. Numerical simulations and 3D MEMs enable predictions from operational plans and data sets; however, without the benefit of CO_2 injection histories or plume monitoring to further validate and calibrate models, uncertainty ranges with predictions remain wide. Since most CO_2 projects have extensive data collection and monitoring programs planned, over time the uncertainty associated with predictions will decrease.

The results of the geomechanical case study for the scenarios investigated suggest acceptable risks are posed to the integrity of the uppermost seal under the effects of pressure increase, buoyant forces from injected CO_2 in multiple intervals, or rock expansion and compression due to pressure and temperature effects during the simulated stacked storage operation. Similarly, the results suggest acceptable risks are posed to the interburden when the same effects are considered. In the scenarios investigated, the interburden thickness was great enough and petrophysical properties (e.g., porosity and permeability) were low enough that neither fluid migration nor pressure buildup would have any significant effect on interference between the injection zones. Situations are conceivable for instances of significantly thinner interburden or interburden with higher petrophysical properties that injected CO_2 could move or cause pore pressure interference from one stacked reservoir to another, lending support to the importance of conducting numerical simulations to understand such phenomena.

The authors acknowledge that this case study was focused on one site and a limited number of scenarios, but some inferences can be drawn about future potential stacked storage scenarios in other locations. The simulated CO_2 injection scenarios investigated here assumed maximum injection rates (e.g., BHP-constrained injection pressures, limited at 90% of fracture pressure in the injection intervals). Reservoir intervals had relatively high porosity and permeability characteristics, allowing lateral fluid migration and pressure dissipation to occur with relative ease. Also, in the scenarios analyzed here, the interburden thickness and associated petrophysical properties were effective in keeping injected CO_2 and associated pressure changes contained within the intended injection intervals. Future potential stacked storage scenarios with similar reservoir and interburden characteristics (e.g., thickness and petrophysical properties) would be expected to have similar results and relatively low risk of interference between injection intervals, even at maximum injection rates permissible. The risks posed by containment and potential interference between injection intervals would be expected to be further reduced in future potential

stacked storage scenarios where injection rates and injection well BHPs are lower than maximum permitted values. However, future potential stacked storage scenarios with much lower ranges of petrophysical properties in the intended injection intervals would be expected to have a much more localized pressure buildup, creating a relatively higher risk of CO_2 migration and pressure buildup in seals and interburden. Also, this study assumed relatively simple geologic characteristics, without faulting or fractures, and the results may be considered transferable to other stacked storage scenarios with a simple geologic structure. In scenarios with a complex structure, faults and fractures, and greater heterogeneity in associated in situ stresses will yield different results, even if similar reservoir, interburden, and operational characteristics are assumed.

Critically stressed faults and natural fractures have potential for reactivation and pose risk for unintended fluid migration within interburden and confining zones. Injection well operational constraints include using a maximum BHP limit not to exceed 90% of fracture propagation pressure for reservoirs during CO_2 injection, intended to avoid opening existing or initiating new faults and fractures. In the absence of site-specific information such as mini-frac data to establish a firm Shmin value by zone and carry out critical stress analyses of faults and fractures, a generic and conservative fracture pressure gradient (e.g., 0.8 psi/ft) may be used to determine a maximum BHP constraint. From this case study, effective stress changes, Mohr–Coulomb failure modes, and thermal stress have the greatest effects near wellbores, with the understanding that the greatest changes in pressure and temperature will occur at the injection wells. In lieu of assuming a generic fracture pressure gradient, a recommendation for safe and successful injection well operation is that site-specific information is generated regarding fracture pressure and natural fracture vulnerability. Of particular importance for increased understanding of geomechanical risks is information regarding fracture behavior in response to near-wellbore stress evolution, including thermal effects, expected during CO_2 injection for reservoir, interburden, and upper confining zones.

Such information is invaluable for two reasons. First, in instances where fracture initiation or fracture reactivation pressure is unexpectedly low and/or natural faults and fractures are critically stressed, site-specific information will help inform an appropriate (lowered) injection rate and maximum BHP to avoid unintended fluid migration, alleviate the potential of slippage and/or induced seismicity, and ensure containment of fluids within intended storage intervals occurs in accordance with an approved permit for operation. Secondly, site-specific information showing that natural faults and fractures are not critically stressed and/or fracture pressure is higher than an assumed generic or calculated conservative gradient can support a recommendation for higher injection rates and maximum BHP constraints. In this scenario, and if approved by the regulatory entity, an operator would be expected to inject greater quantities of CO_2, with potentially greater economic benefits, while having confidence in operating a safe, successful, and permanent storage project.

Temperature and thermal stress modeling should also be expanded to assess variability in injection fluid temperature, convection, and vertical conduction and to consider near-wellbore enhancement of permeability due to thermal effects during the CO_2 injection period. Because the variation of temperature between injected CO_2 and formation fluid is predominantly near injection wellbores, local grid refinement around the injection wells is also recommended to determine the dependency of thermal stress evolution on cell size and distance from injection wells. Also,

managing constant temperature at the injection wellbore is challenging from an operational perspective because of seasonal changes in temperature and heat transfer occurring while CO_2 moves through casing or tubing. Additional studies under varying operational and thermodynamic conditions are recommended (e.g., constant injection rate with varying temperature at the injection wellbores, cyclic injection rate with varying temperature at the injection wellbores, CO_2 phase change at the injection wellbores).

Postfailure behavior (e.g., mechanical behavior after rock starts to fail or yield plasticly), including location and timing, should be considered if failures are expected, with the potential to provide leakage pathways for injected CO_2. This process requires more sophisticated numerical analysis than in the current workflow and should include coupling between pore pressure and stress-activated pathways. Also, additional laboratory core measurements to test for plastic behavior after rock begin to yield will be needed to better calibrate 3D MEM simulations.

If seismic data are available and converted to rock physics volumes (i.e., density, Young's modulus, Poisson's ratio volumes), these inputs can be utilized to calibrate 3D MEMs. 3D seismic can enable mapping of existing structural features, while discrete fracture network models, framed by kinematic fault stress models and calibrated by image log interpretations, enable modeling of natural fracture swarms and orientations which can be incorporated in geologic models. The characterized fault and fractures have potential to affect fluid migration and pressure buildup or represent locations where changing stresses may be most likely to result in movement or slippage. Also, CO_2 storage performance monitoring 4D seismic data during the injection period can be a monitoring tool for CO_2 plume movement, pressure changes, and stress evolution during the injection process. As 4D seismic data are updated at a certain time step, the 3D MEM can be updated for an improved understanding of the subsurface and CO_2 performance predictions.

Interferometric synthetic aperture radar (InSAR), which is a prominent way to measure changes in land surface altitude using radar signals from Earth-orbiting satellites, can be integrated with a 3D MEM. InSAR data can be utilized to measures ground surface movement due to CO_2 injection and pressure buildup in the scale of millimeters in ideal conditions Time-lapse InSAR measurements can be used for calibrating a 3D MEM during the CO_2 injection period.

Computational requirements in completing 3D MEMs are high, with coupled fluid flow and geomechanics modeling demanding additional computational requirements; however, modeling times can be reduced with the use of cloud computing with adequate nodes. To compare, a basic 3D MEM test case designed for performance tracking took 72 hours to run on an 18-core desktop and ran in 15 hours on a 3D MEM-optimized cloud instance with 96 cores. The time savings per case is also compounded by the ability to run multiple instances at once, provided budget allows for the renting of additional cloud resources. Plans to add 3D fault kinematic analysis and discrete fracture network modeling to characterize critical stressed faults and fracture networks in CO_2 storage complexes will require a stepwise increase in required computational power or run times for coupled-flow numerical simulation and 3D MEMs.

SUMMARY AND CONCLUSION

The PCOR Partnership region has many opportunities for stacked storage in deep saline storage complexes, with additional EOR options in hydrocarbon-bearing formations, depleted reservoirs, and unconventional reservoirs. Projects within the Powder River Basin, Williston Basin, Denver–Julesburg Basin, and Alberta Basin were reviewed in Belobraydic and others (2021) for stacked storage potential within deep saline aquifers, while the oil and gas industry and academia have published numerous papers and reports on existing hydrocarbon-bearing EOR projects and unconventional reservoirs. In general, the saline reservoirs with the greatest dedicated storage potential in the PCOR Partnership region are mostly sandstone, but range in number, depth, thickness, and vertical separation between stacked reservoirs.

This case study evaluated the combined stresses and pore pressure changes associated with the injection of significant volumes of CO_2 in a stacked storage configuration. A workflow was implemented to analyze geomechanical impacts and stresses on the interburden between pressured storage units as well as the uppermost confining layer. The workflow passed through several modeling steps by first creating a geologic model of the stacked storage reservoirs, then numerical simulations of CO_2 injection into the reservoirs and, finally, geomechanical simulation using MEMs.

The geologic model provided the initial conditions of the stacked Inyan Kara and Broom Creek Formations with the total stratigraphic overburden within the model. The model provided lithofacies and petrophysical properties for the reservoirs, interburden, upper confining zone, and overburden. The initial porosity, permeability, temperature, and pressure were modeled to create an approximation of the eastern Williston Basin for numerical simulations and geomechanical modeling.

Three scenarios were selected for numerical simulation to test the effects of injecting the maximum operational volume of CO_2 into a stacked storage configuration of the Inyan Kara and Broom Creek Formations for 20 years: stand-alone Inyan Kara injection, stand-alone Broom Creek injection, and simultaneous Inyan Kara and Broom Creek injection with two separate wells. The simultaneous injection provided similar injected CO_2 volume and pore pressure results for each formation compared to the stand-alone cases. All three numerical simulations demonstrate no interconnectivity between the two reservoirs, and injected CO_2 remained contained within the reservoirs. The pore pressure results from each time step and each case were used in geomechanical modeling.

1D MEMs and 3D MEMs were completed as part of the geomechanical investigation. 1D MEMs were completed for four wells to identify pore pressure, elastic mechanical constitutive properties, overburden stress, maximum horizontal stress, and minimum horizontal stress for the initial conditions along the wellbores. Two of the wells were selected, based on proximity to simulated CO_2 injection and data quality, to be used as initial stress condition calibration for the 3D MEM. After calibrating the conditions in the 3D MEM to the 1D MEM results, each of the injection scenarios were simulated over the 20-year CO_2 injection period to determine the effective stress evolution, thermal stress generation, and Mohr–Coulomb failure mode prediction of the injection and confining zones for each time step.

For the given geologic stacked storage setting, CO_2 injection scenarios, and 3D MEM assumptions, all results demonstrate geomechanical isolation and no pressure communication between the Inyan Kara and Broom Creek Formations. No geomechanical failures are observed in the interburden or the upper confining zone. The effective stress evolution during the 20-year injection period for all cases confirms the lack of communication. Mohr–Coulomb failure mode classification predictions and thermal stress generated remain isolated to cells adjacent to CO_2 injection wells within the models.

Well logs, along with direct pressure measurements and core data, allow for good control on current stress conditions for planned injection reservoirs. Adding laboratory measurements for postfailure (e.g., plastic) behavior will allow for better calibration for stress evolution, especially between and pore pressure and stress-activated pathways. Numerical simulations and 3D MEMs enable predictions, in most cases, without the benefit of CO_2 injection histories or plume monitoring that could be used to further validate and calibrate models. CO_2 storage performance-monitoring tools (e.g., 4D seismic, InSAR) will provide additional locations and timing for calibration points and reservoir conditions during injection.

RANKING CRITERIA FOR THE DEVELOPMENT OF A RISK PROFILE

Risk assessment for storage projects is an iterative process of identifying, analyzing, and evaluating individual project risks, which enables project developers to proactively plan and implement mitigation strategies to address individual risk scenarios (Ayash and others, 2016; Azzolina and others, 2017). The general guidelines for executing a risk assessment are presented in ISO 31000 (ISO, 2009), and were adapted to storage projects in ISO 28914 (ISO, 2017) and the EERC's *Best Practices Manual for Subsurface Technical Risk Assessment of Geologic CO_2 Storage Projects* (Azzolina and others, 2017). The four main components to risk assessments for storage projects include i) establish the context, ii) risk identification, iii) risk analysis, and iv) risk treatment. Therefore, the list of site characterization data needs summarized below provides an initial starting point for establishing the context and the risk identification components of the risk assessment and can be utilized by subject matter experts and other project stakeholders developing their own site-specific risk assessments. The results of this stacked storage and geomechanical study were used to inform a list of site characterization data needs that can provide the technical basis of a risk assessment for candidate stacked storage projects.

Site Characterization Data Needs

<u>Overburden and Interburden Layers</u>

- Overburden and interburden thickness – because of the inherent challenges in predicting sealing characteristics away from the wellbore because of potential facies or structural changed, a greater thickness will generally reduce the risk of geomechanical failure

- Dominant lithology and rheology

- Lithology-calibrated thermal conductivity of confining zones for temperature-related thermal stress changes (e.g., permeability hysteresis) near and far from wellbore

- Mechanical stratigraphy, e.g., stress regime, stress directions, and rock strength by layer

- Fracture gradient of overburden and interburden
  - Sealing capacity (e.g., mercury injection capillary pressure profile and capillary entry pressures)

Injection Zones

- Dominant lithology and rheology

- Lateral and vertical continuity and understanding of facies and variations

- Present-day pore pressure and temperature

- Mechanical stratigraphy, e.g., stress regime, stress directions, and rock strength by layer

- Fracture gradient

- Lithology-calibrated thermal conductivity of injection zones for temperature-related thermal stress changes (perm hysteresis, etc.) near and far from wellbore

- Thickness, reservoir characteristics, and effective net-to-gross and Kv/Kh to enable modeling and prediction of fracture gradient failure in response to injection

Faults and Fractures

- Tectonic regime and uplift and denudation history to fault and fracture populations, azimuths and associated respective timing in context

- Nature and occurrence of faulting and fracturing by overburden, interburden, and injection zones; interpretation of dominant structural style

- 3D fault kinematic analysis carried out if fault and fractured determined to be important and a controlling element of the storage complex

- Mohr–Coulomb-based critical stress analysis of faults and fractures to characterize the potential for conduction of fluids in response to injection and/or induced seismicity

Risk Management and Mitigation

The site characterization data are to be utilized by subject matter experts and other project stakeholders to develop a set of potential risk scenarios that describe mechanisms for geomechanical failures of the storage complex and the potential scenarios that could occur as a result. The means and methods previously discussed (e.g., static geologic model, dynamic numerical simulation, and mechanical earth modeling) would then be used to score and rank the risk scenarios to identify a high-graded list of critical risks. The risks will be ranked from critical, short-term risks where risk mitigation is required immediately, to low risks where no immediate action is required but monitoring is necessary. As the project progresses and additional data are

acquired, the CO_2 storage manager may require an update of the risk scenario rankings to inform operational decision-making. Several geomechanical risks, risk management, and risk mitigation items were identified:

- Establish effective CO_2 injection containment sequencing to ensure stacked storage optimization by using a staged approach to ensure integrity of all planned injection zone(s) to understand and measure the dynamic nature of the injected and containment zones throughout the life of the project.

- Data acquisition plans should be designed to inform decisions by impacting known pre-project subsurface technical risk profiles and reduce critical uncertainties to allow robust analyses to be carried out as a project progresses.

- A robust and focused MVA plan is essential to inform decisions on expanding the program to a second or third injection zone in a stacked scenario.

RECOMMENDATIONS FOR FUTURE INVESTIGATIONS

The workflow in this case study was used to assess geomechanical impacts and stresses for CO_2 storage in a simulated stacked storage operation targeting the Inyan Kara and Broom Creek Formations. Future PCOR Partnership activities could be focused on generating additional site-specific characterization data needed for future geomechanical investigations targeting other reservoirs and across a broader portion of the PCOR Partnership region. As more publicly available modern characterization and monitoring data are collected at operational CCS sites (e.g., InSAR, 3D seismic data, and 4D [time-lapse] seismic data), detailed site-specific geomechanical investigations can be conducted with greater accuracy and decreased uncertainty in results.

A recommendation for future PCOR Partnership geomechanics research is conducting additional scenarios that test ranges of stacked storage geomechanical sensitivities that are geologic and operational. Geologic sensitivities would include interburden thickness, depth (including associated temperature and pressure conditions in the reservoirs, interburden, and seals), lithology for reservoir, interburden, and seals, natural fault and fracture characteristics and density, and petrophysical properties for reservoir, interburden, and seals. Operational sensitivities would include injection rate and pressure constraints, boundary conditions (e.g., open versus closed), and well construction (e.g., vertical versus horizontal wells). Additional coupled fluid simulation, geochemistry, and geomechanical studies to investigate changes in mechanical integrity during stacked storage are recommended to address expected changes in mineral composition occurring during exposure to CO_2.

To test geomechanical sensitivities, it is recommended that geologic models and numerical simulations be varied to test ranges of scenarios within the subsurface, consider wider operational data ranges, and be designed to minimize 3D MEM simulation computational intensity and run time. However, and while keeping computational intensity in mind, future investigations should consider local grid refinements adjacent to the injection wells to better estimate thermal stress propagation profiles away from the injection wells, because the shear and, more particularly, the

tensile failures happening immediately around the injection wellbores could provide an improvement to permeability and injectivity of CO_2 (e.g., negative skin values), as also observed in Jiang and others (2017). Continued development of this workflow is recommended to integrate a more comprehensive set of inputs (i.e., faulting, natural fractures, vertical conduction, convection) and processes (i.e., thermal stress permeability enhancement, stress induced pore pressure influences, and post-failure behavior) known to exist within storage complexes.

These recommendations aim to build on the incremental learnings of this study. Application and customization of this workflow to test a greater number of scenarios will help generate additional learnings transferable to a wider portion of the PCOR Partnership region and other locations with similar geologic characteristics. Insights gained from using the recommended geomechanical sensitivities found in this case study can be used to inform operational parameters needed for certain geologic scenarios to limit unintended geomechanical effects during injection. Conducting these investigations will help to better understand the technical challenges and risks posed by geomechanical effects during stacked storage operations while providing actionable information to stacked storage site operators to ensure safe and successful results.

REFERENCES

Aadnøy, B. and Looyeh, R., 2019, Petroleum rock mechanics—drilling operations and well design (2d ed.).

Ayash, S.C., Nakles, D.V., Peck, W.D., Sorensen, J.A., Glazewski, K.A., Aulich, T.R., Klapperich, R.J., Azzolina, N.A., and Gorecki, C.D., 2016, Best practice for the commercial deployment of carbon dioxide geologic storage—adaptive management approach: Plains CO_2 Reduction (PCOR) Partnership Phase III draft Task 13 Deliverable D102/Milestone M59 for U.S. Department of Energy National Energy Technology Laboratory Cooperative Agreement No. DE-FC26-05NT42592, Grand Forks, North Dakota, Energy & Environmental Research Center, August.

Azzolina, N.A., Nakles, D.V., Ayash, S.C., Wildgust, N., Peck, W.D., and Gorecki, C.D., 2017, PCOR Partnership best practices manual for subsurface technical risk assessment of geologic CO_2 storage projects: Plains CO_2 Reduction (PCOR) Partnership Phase III Task 9 Deliverable D103 for U.S. Department of Energy National Energy Technology Laboratory Cooperative Agreement No. DE-FC26-05NT42592, EERC Publication 2017-EERC-10-21, Grand Forks, North Dakota, Energy & Environmental Research Center, August.

Bader, J.W, 2017, Sequence stratigraphy of the Inyan Kara Formation, North Dakota: North Dakota Geological Survey, Search and Discovery Article No. 51414.

Belobraydic, M.L., Richards, T.L., Pekot, L.J., Stevens, C.R., Feole, I.K., Warmack, M.P., Regorrah, J.G., Burnison, S.A., Meyer, J.A., Klapperich, R.J., Peck, W.D., Bosshart, N.W., and Connors, K.C., 2021, Technical approaches to stacked storage: Deliverable D3.A for U.S. Department of Energy National Energy Technology Laboratory Cooperative Agreement No. DE-FE0031838, North Dakota Industrial Commission, Grand Forks, North Dakota, Energy & Environmental Research Center, October, 44 p.

Bergman, T.L., Lavine, A.S., Incropera, F.P., and DeWitt, D.P., 2017, Fundamentals of heat and mass transfer (8th ed.): Wiley.

Computer Modelling Group, 2021a, GEM (compositional and unconventional simulator) manual.

Computer Modelling Group, 2021b, Winprop (fluid property characterization tool) manual.

Dusseault, M., 2019, Introduction to petroleum geomechanics: https://isrm.net/page/show/994 (accessed 2022).

Fjaer, E., Holt, R.M., Horsrud, P., and Raaen, A., 2008, Petroleum related rock mechanics (2d ed.): Elsevier.

Hovorka, S.D., 2013, CCU&S via stacked storage—case studies from CO_2-EOR basins of the United States: Energy Procedia, v. 37, p. 5166–5171. DOI: 10.1016/j.egypro.2013.06.432.

Hovorka, S.D., Denson, S.M., Doughty, C., Freifeld, B.M., Sakurai, S., Daley, T.M., Kharaka, Y.K., Holtz, M.H., Trautz, R.C., Nance, H.S., Myer, L.R., and Knauss, K.G., 2006, Measuring permanence of CO_2 storage in saline formations—the Frio experiment: Environmental Geosciences, v. 13, p. 105–121. DOI: 10.1306/eg.11210505011.

International Organization for Standardization, 2009, Risk management—principles and guidelines: ISO. 31000:2009(E).

International Organization for Standardization, 2017, Carbon dioxide capture, transportation, and geological storage—geological storage: ISO 27914:2017.

Nghiem, L., Shrivastava, V.K., Tran, D., Kohse, B., Frederick, H., Hassam, M., and Yang, C., 2009, Simulation of CO_2 storage in saline aquifers: Paper presented at the SPE/EAGE Reservoir Characterization and Simulation Conference, Abu Dhabi, UAE, October. https://doi.org/10.2118/125848-MS.

Jiang, T., Pekot, L.J., Jin, L., Peck, W.D., Gorecki, C.D., and Worth, K., 2017, Numerical modeling of the Aquistore CO_2 storage project: Energy Procedia, v. 114, p. 4886–4895. DOI: 10.1016/j.egypro.2017.03.1630.

Peck, W.D., Azzolina, N.A., Nakles, D.V., Glazewski, K.A., Klapperich, R.J., Crocker, C.R., Oster, B.S., Daly, D.J., Livers-Douglas, A.J., Butler, S.K., Smith, S.A., Botnen, B.W., Feole, I.K., He, J., Dotzenrod, N., Salazar, A.Y., Patil, S.B., and Crossland, J.L., 2020, North Dakota integrated carbon storage complex feasibility study: Final report for U.S. Department of Energy National Energy Technology Laboratory Cooperative Agreement No. DE-FE0029488, North Dakota Industrial Commission, Grand Forks, North Dakota, Energy & Environmental Research Center, March.

Peng, D.-Y., and Robinson, D.B., 1976, A new two-constant equation of state: Industrial & Engineering Chemistry Fundamentals, v. 15, p. 59–64.

Python, 2021, www.python.org/ (accessed 2021).

Rygh, M.E., 1990, The Broom Creek Formation (Permian), in southwestern North Dakota—depositional environments and nitrogen occurrence [Master's thesis]: University of North Dakota, p. 189.

Sorensen, J.A., Bailey, T.P., Smith, S.A., Gorecki, C.D., Fischer, D.W., Peck, W.D., Steadman, E.N., and Harju, J.A., 2009, CO_2 storage capacity estimates for stacked brine-saturated formations in the North Dakota portion of the Williston Basin: Energy Procedia, v. 1, no. 1, p. 2833–2840. DOI: 10.1016/j.egypro.2009.02.056.

Schlumberger, 2020a, Petrel 2020.5: Petrel E&P software platform.

Schlumberger, 2020b, TechLog 2020.1: TechLog petrophysical software platform.

Schlumberger, 2020c, Visage 2020.5: Visage reservoir geomechanics simulator.

U.S. Department of Energy National Energy Technology Laboratory, 2015, The 2015 United States carbon utilization and storage atlas—Atlas V (5th ed.): www.netl.doe.gov/sites/default/files/2018-10/ATLAS-V-2015.pdf (accessed March 2022).

U.S. Environmental Protection Agency, 2018, Geologic sequestration of carbon dioxide: Underground injection control (UIC) program Class VI implementation manual for UIC program directors, Office of Water, EPA 816-R-18-001, January www.epa.gov/sites/default/files/2018-01/documents/implementation_manual_508_010318.pdf (accessed March 2022).

Ziebarth, H.C., 1972, The stratigraphy and economic potential of Permo-Pennsylvanian strata in southwestern North Dakota [Ph.D. dissertation]: University of North Dakota, 414.